

Summer 8-2018

## Parametric Study of Aerodynamic Performance of an Airfoil with Active Circulation Control Using Leading Edge Embedded Cross-Flow Fan

M.A. Qayyum Mazumder  
*Embry-Riddle Aeronautical University*

Follow this and additional works at: <https://commons.erau.edu/edt>



Part of the [Aerodynamics and Fluid Mechanics Commons](#)

---

### Scholarly Commons Citation

Mazumder, M.A. Qayyum, "Parametric Study of Aerodynamic Performance of an Airfoil with Active Circulation Control Using Leading Edge Embedded Cross-Flow Fan" (2018). *Doctoral Dissertations and Master's Theses*. 422.

<https://commons.erau.edu/edt/422>

This Thesis - Open Access is brought to you for free and open access by Scholarly Commons. It has been accepted for inclusion in Doctoral Dissertations and Master's Theses by an authorized administrator of Scholarly Commons. For more information, please contact [commons@erau.edu](mailto:commons@erau.edu).

PARAMETRTIC STUDY OF AERODYNAMIC PERFORMANCE OF AN AIRFOIL  
WITH ACTIVE CIRCULATION CONTROL USING LEADING EDGE EMBEDDED  
CROSS-FLOW FAN

A Thesis

Submitted to the Faculty

of

Embry-Riddle Aeronautical University

by

M A Qayyum Mazumder

In Partial Fulfillment of the

Requirements for the Degree

of

Master of Science in Aerospace Engineering

August 2018

Embry-Riddle Aeronautical University

Daytona Beach, Florida

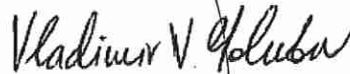
PARAMETRTIC STUDY OF AERODYNAMIC PERFORMANCE OF AN AIRFOIL  
WITH ACTIVE CIRCULATION CONTROL USING LEADING EDGE EMBEDDED  
CROSS-FLOW FAN

by

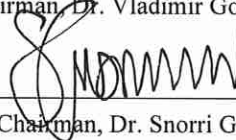
M A Qayyum Mazumder

A Thesis prepared under the direction of the candidate's committee chairman, Dr. Vladimir Golubev and Dr. Snorri Gudmundsson, Department of Aerospace Engineering, and has been approved by the members of the thesis committee. It was submitted to the School of Graduate Studies and Research and was accepted in partial fulfillment of the requirements for the degree of Master of Science in Aerospace Engineering.

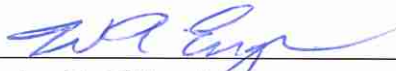
THESIS COMMITTEE



Chairman, Dr. Vladimir Golubev



Co-Chairman, Dr. Snorri Gudmundsson



Member, Dr. William Engblom



Graduate Program Coordinator, Dr. Magdy Attia

9/14/18

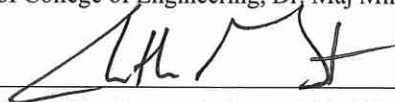
Date



Dean of College of Engineering, Dr. Maj Mirmirani

9/17/18

Date



Vice Chancellor, Academic Support, Dr. Christopher Grant

9/17/18

Date

## ACKNOWLEDGMENTS

I would like to express my gratitude to Dr. Vladimir Golubev, Dr. Snorri Gudmundsson and Dr. William Engblom for their guidance and support throughout the thesis. Without their insight, the completion of this thesis would not be possible.

I would like to thank Mr. Darrell Stevens for his invaluable support in developing the CAD models for this thesis. Mr. Stevens taught me the necessary CAD modelling for this thesis, and it was only after his guidance the thesis began to fall in place.

I would like to thank my fellow classmate, Mr. Stanislav Karpuk, for helping me getting started with the simulations and for his overall advice in the subject matter of this thesis.

I am grateful to Dr. Jayathi Raghavan for teaching me how regression equations can be implemented in my thesis to answer certain questions arising from this research.

I am grateful to the Department of Mathematics at Embry-Riddle Aeronautical University for their support in continuing my graduate studies.

I would like to thank my friends Taohid Latif, Bryan Rabbitt and Sujit Roy, who have helped me tremendously in times of need while I was pursuing my studies.

I am eternally grateful to my mother Hosne Ara Mazumder, father M A Gaffur Mazumder, Uncle Abdul Jabbar Mazumder and his family, Uncle Mostafizur Rahman, my brothers Abdul Kader and Karim Mazumder, sister-in-law Afroza Haque, and my roommate Naveen for providing continuous support and encouragement all throughout.

I am grateful to thank all staff and faculty who contributed to development and support of the VEGA cluster. This project would not be possible without strong computational power available in ERAU.

*“What man is a man who doesn’t make the world better?”*

- Kingdom of Heaven (2005 film)

LIST OF TABLES.....	vi
LIST OF FIGURES .....	vii
SYMBOLS.....	ix
ABBREVIATIONS .....	x
1. Introduction .....	1
1.1. Previous Work.....	2
1.2. Physics of the System.....	5
1.2.1. Aerodynamics of Cross-Flow Fan.....	5
1.2.2. Active Boundary Layer Control .....	7
1.2.3. Free Shear Layer.....	8
1.3. Objective of Current Research.....	9
2. Fan-Wing Model .....	11
3. Computational Setup.....	13
3.1. Grid.....	13
3.1.1. Grid Sensitivity Analysis .....	14
3.2. Numerical Solver and Scheme .....	16
4. Results and Analysis .....	18
4.1. Clean Case .....	18
4.2. Number of Blades.....	20
4.3. Blade Pitch Angle.....	23
4.4. Fan Diameter Ratio .....	26
4.5. Pressure Side Slat Opening.....	29
4.6. Suction Side Slat Opening .....	32
4.7. Regression Analysis .....	34
4.8. Effect of Thickness on Circulation Control .....	40
5. Conclusion.....	41
6. Recommendations .....	42
REFERENCES .....	43

## LIST OF TABLES

Table 4-1 Results from Number of Blades Study .....	20
Table 4-2 Results from Blade Pitch Angle Study .....	24
Table 4-3 Results from Fan Diameter Ratio Study .....	27
Table 4-4 Results from Bottom Slat Opening Study .....	29
Table 4-5 Results from Top Slat Opening Study .....	32
Table 4-6 Coefficients from regression equation .....	35
Table 4-7 Critical Points obtained from Regression Analysis .....	38
Table 4-8 Results obtained from simulation from regression analysis parameters .....	39
Table 4-9 Comparison between thick and thin airfoil .....	40

## LIST OF FIGURES

Figure 1-1 Flow simulation and cut-way view of cross-flow fan.....	1
Figure 1-2 Cross-flow fan envisioned by Paul Mortier in 1893 .....	2
Figure 1-3 Model and results from Jones' research.....	3
Figure 1-4 Cross-flow fan airfoil geometry by Kummer.....	4
Figure 1-5 Performance comparisons between vortex cavities: total pressure ratio .....	4
Figure 1-6 Three types of blade geometry used by Dr. Kummer .....	4
Figure 1-7 Performance comparison: blade geometry, total pressure ratio .....	5
Figure 1-8 Path-lines through a cross flow fan.....	6
Figure 1-9 Pictorial demonstration of active boundary layer control by blowing.....	7
Figure 1-10 Schematic of boundary layer of a flat plate at zero incidence .....	7
Figure 1-11 Velocity distribution of the boundary layer directly after the jet.....	8
Figure 1-12 Sketch of a plane shear layer.....	9
Figure 1-13 Varying parameters for research .....	9
Figure 1-14 Flow chart of research process.....	10
Figure 2-1 Fan-wing design.....	11
Figure 2-2 Blade design.....	11
Figure 2-3 Blade diameter in inches .....	12
Figure 3-1 Full domain .....	13
Figure 3-2 Rotating region.....	14
Figure 3-3 Structured grid near wall.....	14
Figure 3-4 Fine grid .....	15
Figure 3-5 Coarse grid .....	15
Figure 4-1 NACA 65 <sub>1</sub> -212 Airfoil.....	18
Figure 4-2 Coefficient of Lift vs. Angle of Attack .....	19
Figure 4-3 Coefficient of Drag vs Coefficient of Lift.....	19
Figure 4-4 $C_l$ and $C_p$ vs. Number of Blades .....	21
Figure 4-5 $C_l/C_p$ vs. Number of Blades .....	21
Figure 4-6 $C_d$ vs. Number of Blades .....	22
Figure 4-7 Wall Shear Stress between 24 Blades and 22 Blades .....	23
Figure 4-8 Blade Pitch Angle .....	24
Figure 4-9 $C_l$ and $C_p$ vs. Blade Pitch Angle.....	25



Figure 4-10 $C_l/C_p$ vs. Blade Pitch Angle .....	25
Figure 4-11 $C_d$ vs. Blade Pitch Angle.....	26
Figure 4-12 $C_l$ and $C_p$ vs. Hub/Shroud Ratio.....	27
Figure 4-13 $C_l/C_p$ vs Hub/Shroud Ratio .....	28
Figure 4-14 $C_d$ vs Hub/Shroud Ratio.....	28
Figure 4-15 Pressure Side Slat Opening .....	29
Figure 4-16 $C_l$ and $C_p$ vs. Slat Radius.....	30
Figure 4-17 $C_l/C_p$ vs Slat Radius .....	31
Figure 4-18 $C_d$ vs/ Slat Radius .....	31
Figure 4-19 $C_l$ and $C_p$ vs. Stretch Factor .....	33
Figure 4-20 $C_l/C_p$ vs. Stretch Factor .....	33
Figure 4-21 $C_d$ vs. Stretch Factor.....	34
Figure 4-22 Comparison with number of blades data.....	36
Figure 4-23 Comparison with blade pitch angle data .....	36
Figure 4-24 Comparison with hub/shroud ratio data .....	37
Figure 4-25 Comparison with pressure side slat opening data .....	37
Figure 4-26 Comparison with suction side slat opening data .....	38

## SYMBOLS

$\omega$	angular velocity
$c$	chord
$C_d$	coefficient of drag
$C_l$	coefficient of lift
$C_m$	coefficient of moment
$C_p$	coefficient of power
$\rho$	density
$D$	external diameter of fan
$u_\infty$	free-stream velocity
$y^+$	non-dimensional distance derived from Y
$P$	power
$\tau_{xx}$	shear stress on x plane in x direction
$\tau_{xy}$	shear stress on x plane in y direction
$\tau_{yx}$	shear stress on y plane in x direction
$\tau_{yy}$	shear stress on y plane in y direction
$p$	static pressure
$r^2$	statistical measure of how close the data are to the fitted regression line
$T$	temperature
$k$	thermal conductivity
$t$	time
$T_s$	torque on shaft
$\Delta s$	wall spacing
$u$	x-component of velocity
$v$	y-component of velocity

## ABBREVIATIONS

2-D	two dimensional
3-D	three dimensional
AOA	angle of attack
CAD	computer aided design
CFD	computational fluid dynamics
CFF	cross-flow fan
OFAT	one-factor-at-a-time
RPM	revolutions per minute
SIMPLEC	semi-implicit method for pressure linked equations-consistent

## ABSTRACT

Mazumder, M A Qayyum MSAE, Embry-Riddle Aeronautical University, August 2018.

Parametric Study of Aerodynamic Performance of an Airfoil with Active Circulation Control using Leading Edge Embedded Cross-Flow Fan.

A concept of a cross-flow fan (CFF) embedded near the leading edge of an airfoil to actively control the boundary layer for lift and thrust enhancement has been proposed. The design places a cross-flow fan near the leading edge of an airfoil and flow is drawn in from the pressure side of the airfoil, energized and expelled out to the suction side near the leading edge. This CFF system simulates the active boundary layer control by blowing. The commercial computational fluid dynamics (CFD) code ANSYS Fluent is employed to perform 2-D calculations based on various parameters of the CFF and compared the data with an experimental baseline case found in literature. The effect of number of blades, pressure side slat opening, suction side slat angle, hub-to-shroud ratio and blade pitch angle have on aerodynamic parameters have been investigated. Regression models are established using the acquired data to find combination of parameters for achieving higher circulation control. Unsteady sliding mesh method is used to carry out the numerical simulation. The fan geometry is developed and housed in a NACA 65<sub>1</sub>-212 airfoil. The results of the CFD work show that the jet leaving the fan replaces the boundary layer of the upstream flow with a flow of very high velocity. This high velocity flow causes a higher pressure difference between the suction and the pressure side generating higher lift in the process. The drag of the airfoil is overcome and a net thrust is observed by CFF blowing phenomenon.

## 1. Introduction

Cross-flow fan operate in a different way from conventional turbomachinery in that the suction and discharge of air occur radially. An illustration of the flow field and a cut-way view of cross-flow fan is given in Figure 1-1. The main features of cross-flow fan are the double passage of air across the blades and the formation of eccentric vortex inside the impeller due to the motion of the blades themselves. The fan performance and efficiency is mainly governed by the strength and position of this eccentric vortex (Toffolo, 2004). The flow through a cross-flow fan is identical through the rotational axis, hence a 2-D computational research is sufficient to capture all the relevant physics of the whole 3-D system as well.

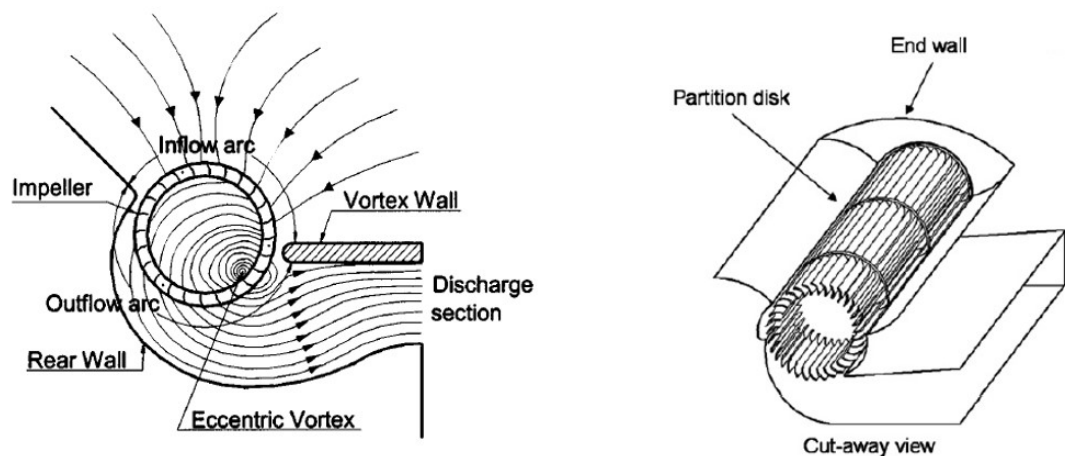


Figure 1-1 Flow simulation and cut-way view of cross-flow fan

Cross-flow fan was first patented by French inventor Paul Mortier in 1893. According to this invention no net centrifugal force is created as the intake and discharge takes place at an equal distance from the axis of rotation. Figure 1-2 shows the cutaway view of a cross-flow fan developed by Mortier (France Patent No. US507445, 1893). The blocks F, which are fixed in chamber, while the wheel revolves, is to guard from the inverse pull from the left portion of the wheel. Mortier noticed that the final speed at K is almost

treble than that of its initial entrance speed at L. Initially the cross-flow fan was designed for ventilation of coalmines. Currently, cross-flow fans are not so widely used in industrial applications but their silent operations makes it suitable for domestic applications such as air-conditioner and air-curtain systems (Kim, Ahn, & Oh, 2005).

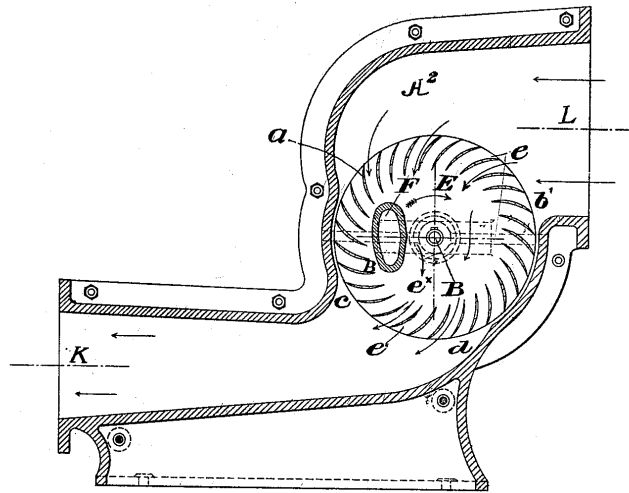


Figure 1-2 Cross-flow fan envisioned by Paul Mortier in 1893

### 1.1. Previous Work

Multiple research has been carried out regarding cross flow fan imbedded in an airfoil for circulation control and/or thrust control. Dornier patented the design of an aircraft that used cross-flow fan embedded within the middle of a conventional airplane wing (USA Patent No. 3,065,928, 1962). Hancock proposed distributing fully embedded cross-flow fans near the trailing edge of a conventional transport aircraft with shafts and couplings connecting them to wing-tip and root-mounted gas turbines (Hancock, 1980).

In 1980's, three additional efforts were made to investigate wing-embedded cross-flow fan propulsion and flow control. The first was by Chawla, who performed a series of wing tunnel tests, which demonstrated the use of CFF for boundary layer control by blowing. Chawla placed the CFF within the middle of a thick airfoil, flow was ducted from

the airfoil pressure surface, through the fan, and exhausted over the suction surface as a jet. This increased the maximum  $C_L$  by delaying stall at high angle of attack (Chawla, 1984). Two subsequent studies attempted to use flow drawn into the fan from leading edge and expelled over the suction surface to provide both thrust and circulation control (Lin, 1986) (Nieh, 1988).

Andria Jones from Naval Postgraduate School carried out numerical and experimental research to determine how much thrust can be generated. The research used a fixed rotor design of 20 blades with 11.08 mm chord length and 3 inches diameter and implementing ANSYS CFX to carry out simulation from 4,000 rpm to 10,000 rpm. Figure 1-3 shows the 2-D model and the thrust results as generated by ANSYS CFX (Jones, 2013).

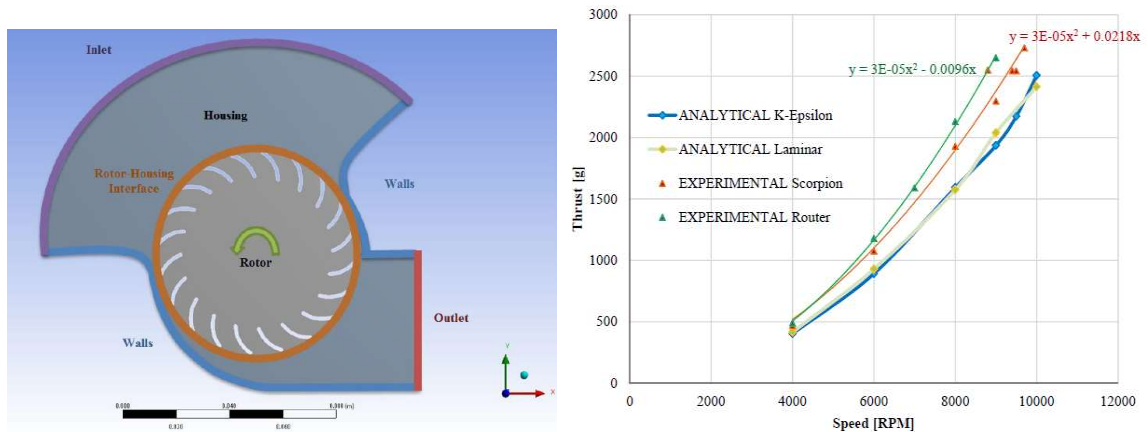


Figure 1-3 Model and results from Jones' research

Kummer from Syracuse University carried out research by placing a cross-flow fan near the trailing edge of a 34% Gottingen 570 airfoil for boundary layer control and thrust generation (Kummer, 2006). Figure 1.4 shows the geometry.

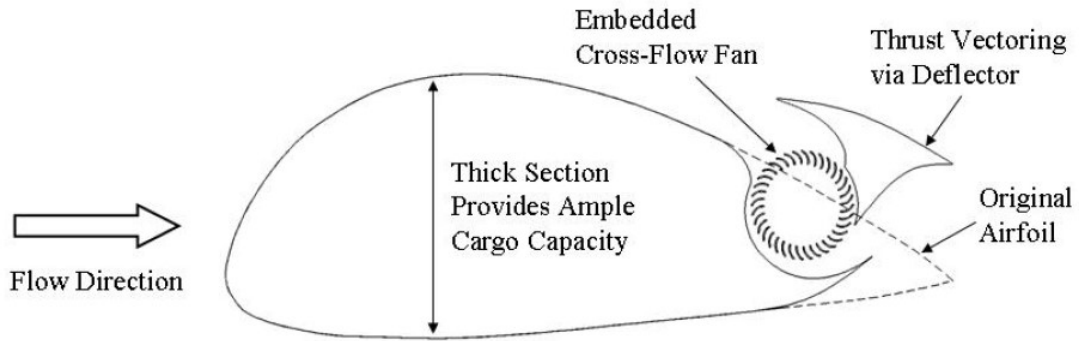


Figure 1-4 Cross-flow fan airfoil geometry by Kummer

Kummer carried out various parametric study by removing the vortex cavity, varying the vortex wall clearance and varying the fan blade geometry.

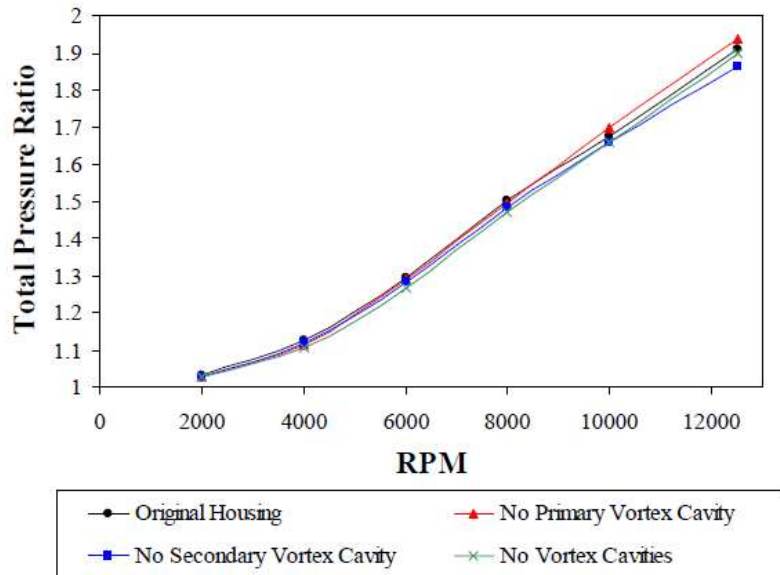


Figure 1-5 Performance comparisons between vortex cavities: total pressure ratio

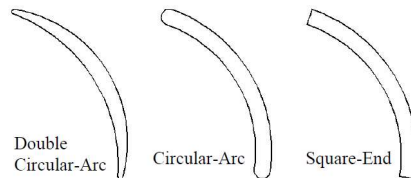


Figure 1-6 Three types of blade geometry used by Dr. Kummer



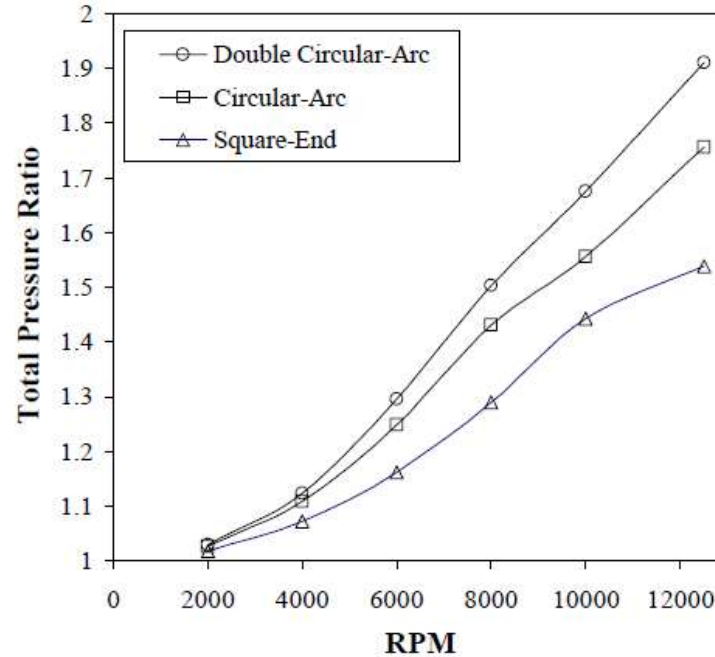


Figure 1-7 Performance comparison: blade geometry, total pressure ratio

From Kummer's research it is established that a double circular arc and no vortex cavity shall be implemented for this research.

## 1.2. Physics of the System

The physics of the fan-wing system can be broken down to three parts: i) aerodynamics of the cross-flow fan ii) active boundary layer control, and iii) free shear layer

### 1.2.1. Aerodynamics of Cross-Flow Fan

The flow field of a cross-flow fan is primarily 2-D, moving perpendicular to the impeller axis. Flow enters the blade in radially inward direction from upstream, passing through the interior of the impeller, and then passes radially outward through the blading a second time. The flow is characterized by the formation of an eccentric vortex that runs

parallel to the rotor axis with rotation in the same direction. Figure 1-8 shows the instantaneous path-lines through the cross flow fan.

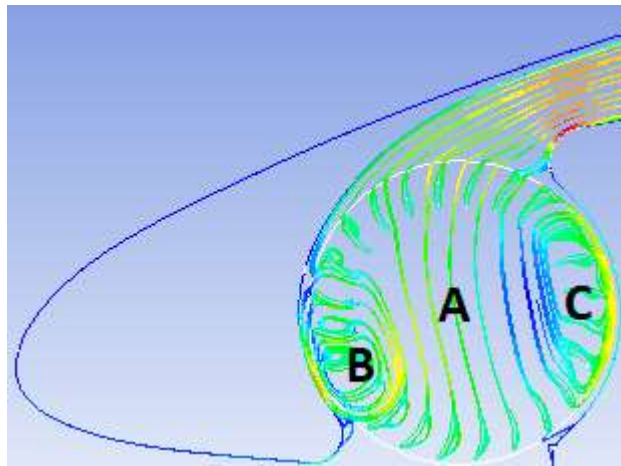


Figure 1-8 Path-lines through a cross flow fan

The flow within the region can be divided into three regions that may be analyzed independently. The three flow regions are designated A, B and C as shown in Figure 1-8. Region A represents the main through-flow in the fan and is where the most of the useful work is done. Two-stage action occurs as the flow passes first through the suction arc blading (first stage) and then through the discharge arc (second stage). The flow contracts as it moves across the impeller producing high velocities at the second stage. The flow leaves the impeller and contracts again as it turns and squeezes around the vortex and exits the fan. The combination of all these effects results in high pressure coefficient capability. Energy transfer in region B is low but is a necessary consequence of the cross-flow phenomenon; however it has little to no effect on the overall performance except with regard to its influence in determining the shape of the through-flow region. Region C represents the eccentric vortex. This region consists of entirely of re-circulating flow, so no useful work is done there and its primary affects are energy dissipation and shaping of region A. In frame of reference of rotating blades, the flow reverses twice per revolution

with blades leading edges becoming trailing edges each time, so regions B and C are fundamentally efficient but unavoidable (Dang & Bushnell, 2009).

### 1.2.2. Active Boundary Layer Control

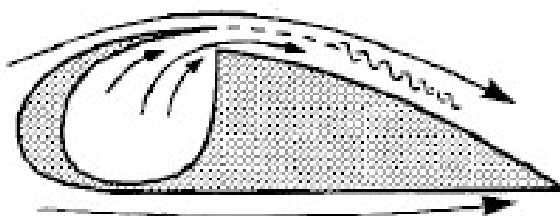


Figure 1-9 Pictorial demonstration of active boundary layer control by blowing

The high velocity jet exiting from the cross-flow fan energizes the boundary layer and enable to sustain larger pressure gradient. The velocity profile at the boundary layer is altered from Figure 1-10 to Figure 1-11 due to the blowing phenomenon.

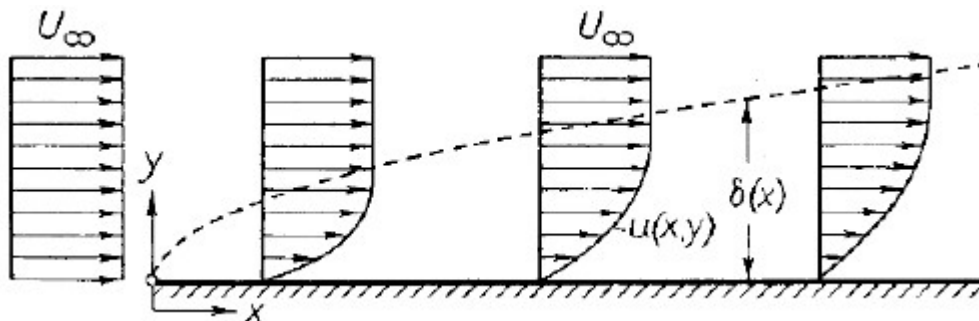


Figure 1-10 Schematic of boundary layer of a flat plate at zero incidence

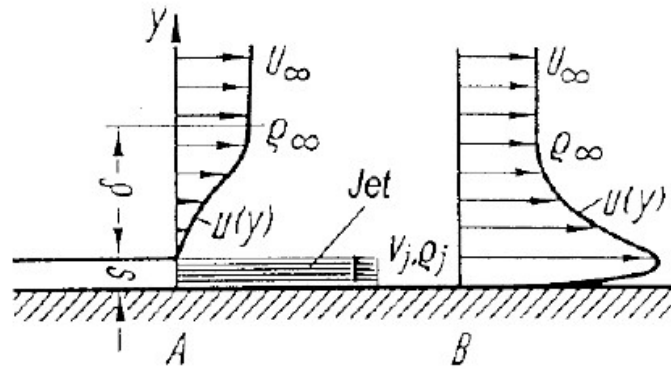


Figure 1-11 Velocity distribution of the boundary layer directly after the jet

As the jet from the fan leaves at A onto the surface of the airfoil it interacts to the slower free stream from the top and result in a velocity profile similar to station B in figure 1.10. The high velocity jet coming from the cross-flow fan decreases the static pressure on the pressure side of the airfoil causing an increases in lift generated (Schlichting & Glaus, 2017).

### 1.2.3. Free Shear Layer

A plane shear layer is formed when the jet leaves the pressure side of the airfoil and interacts with air coming from the suction side. Plane shear layer is formed when two parallel streams of different velocities are separated by a thin plate (ex. trailing edge of an airfoil) and come together as the plate ends. The layer grows from the resulting velocity discontinuity and thickens downstream as shown in Figure 1-12. The free shear layer generate noise and dissipate energy, and are therefore a source of drag of the fan-wing system (Jimenez, 2013).

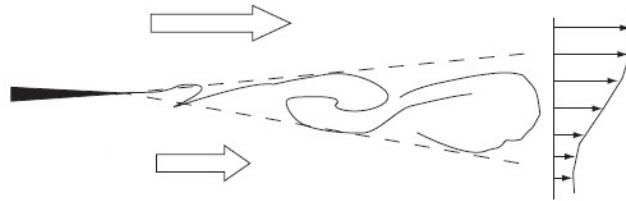
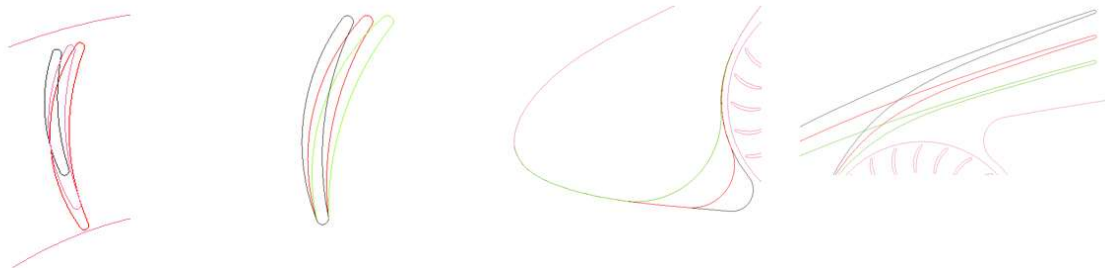


Figure 1-12 Sketch of a plane shear layer

### 1.3. Objective of Current Research

The objective of this research is to observe the change in aerodynamic parameters such as circulation control and thrust control due to changes in various parameters of the embedded cross-flow fan. The parameters to be studied are:

- i. Number of blades
- ii. Blade pitch angle
- iii. Fan diameter ratio
- iv. Pressure side slat opening
- v. Suction side slat opening



i) fan diameter ratio    ii) blade pitch angle    iii) pressure side slat opening    iv) suction side slat opening

Figure 1-13 Varying parameters for research

The computational research is carried out by changing a single parameter at a time and keeping the rest of the parameters constant at a certain value. Since the parameters are interdependent to one another, once sufficient data has been established regression models are generated to combine all the parameters into one equation of circulation control from

where combination of parameters for achieving higher circulation control is obtained by finding the critical points of the regression equation. The stages of the research has been depicted in Figure 1-14.

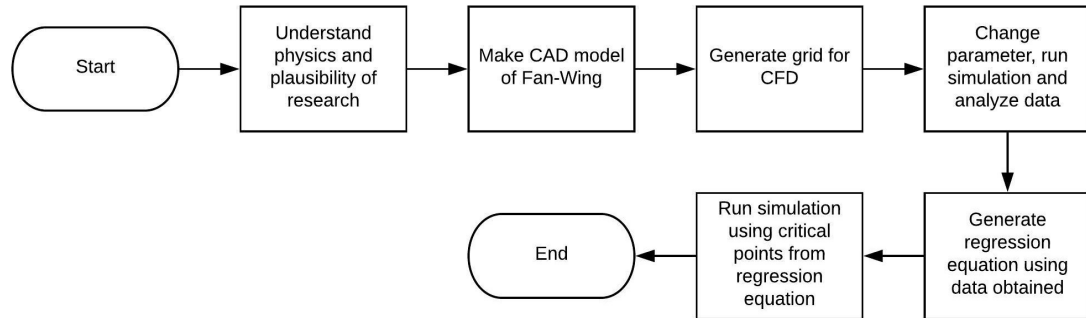


Figure 1-14 Flow chart of research process

## 2. Fan-Wing Model

CATIA, a CAD software is used to generate the fan-wing model. The center of the cross-flow fan is placed at 10% chord of the NACA 65<sub>1</sub>-212 airfoil. The top portion of the nose is created by multiplying the y-coordinates of NACA 65<sub>1</sub>-212 by 1.2. The nose of the airfoil is rotated counter-clockwise by 5° about the fan center to achieve circular flow from the fan. Figure 2-1 is the base design from which parameters are then altered for research.

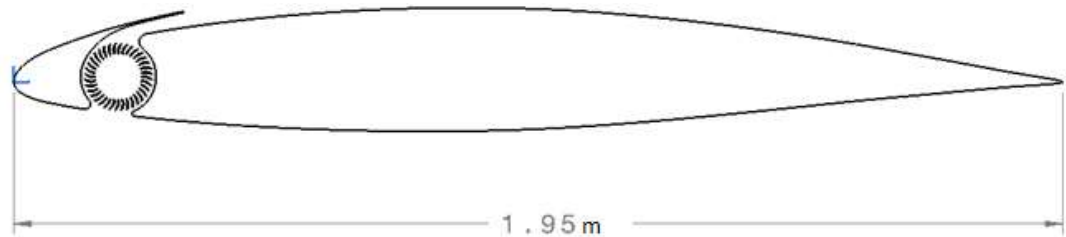


Figure 2-1 Fan-wing design

The vortex wall clearance is set at 10% and inner blade angle set at 90° as suggested by TRANE (TRANE, 2000).

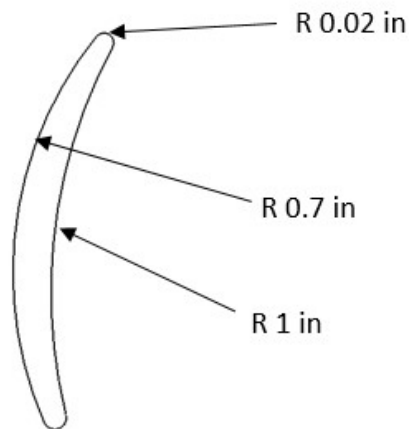


Figure 2-2 Blade design

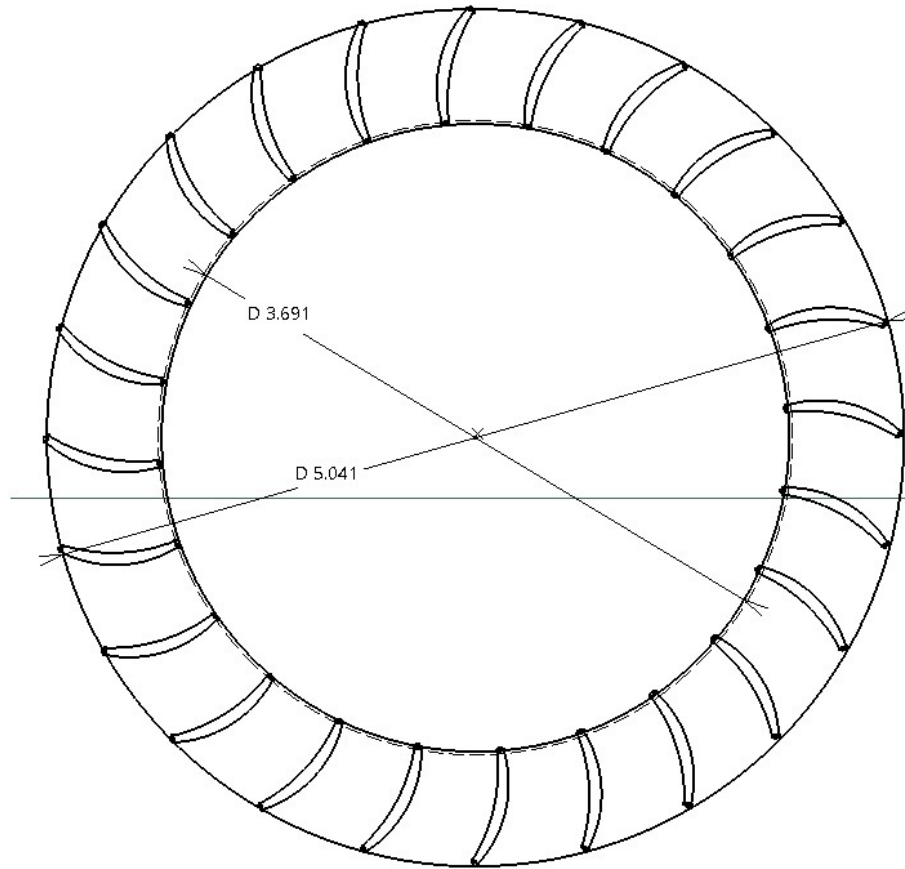


Figure 2-3 Blade diameter in inches



### 3. Computational Setup

#### 3.1. Grid

A hybrid O-grid is generated using Pointwise, a mesh generation software, using  $\Delta s = 0.001$  along the wall. A structured grid of wall spacing of  $1.61575e-05$  normal to the airfoil ensured a  $y^+$  value of 1 based on the boundary conditions. A growth rate of 1.3 is implemented for 13 steps for the structured grid to capture the boundary layer of the airfoil. The far-field extends to 40 chord length. The case with 24 blades, 0.5 inch of bottom slat angle, and 74% of hub-to-shroud ratio has a full domain of 285,385 triangles, 57,720 quadrilaterals. Total cells and points count is 343,105 and 210,130 respectively. The rotating region has 76,937 for this case. Other cases have slightly different number of cells and points but the wall spacing is kept constant.

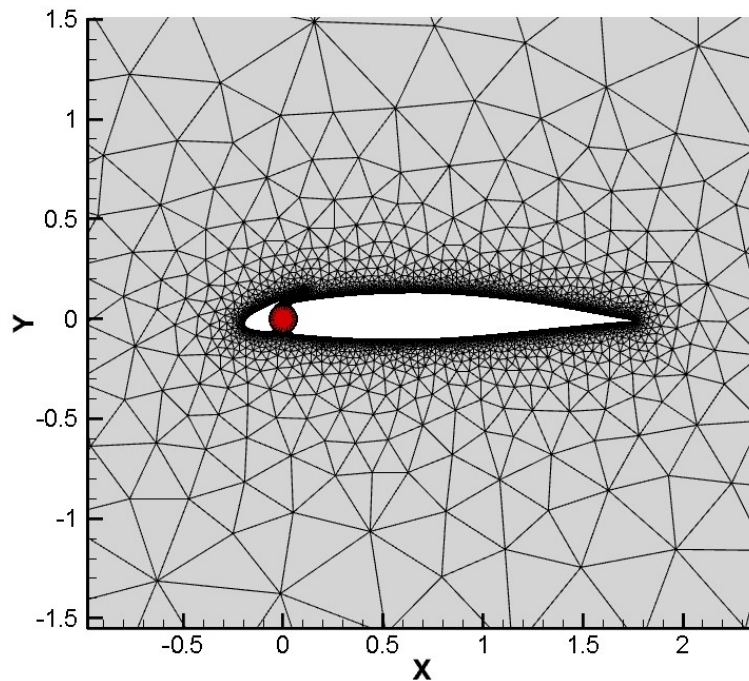


Figure 3-1 Full domain

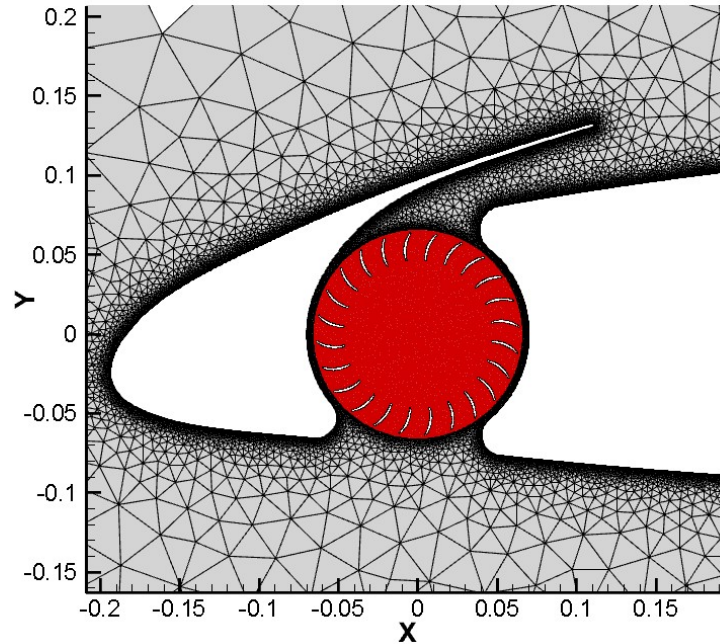


Figure 3-2 Rotating region

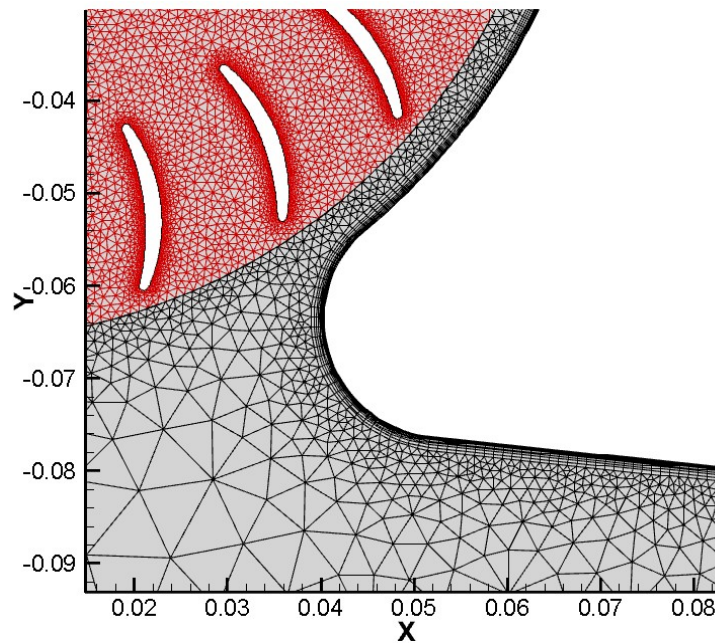


Figure 3-3 Structured grid near wall

### 3.1.1. Grid Sensitivity Analysis

A grid sensitivity analysis was carried out between a coarse grid and a fine grid and the results of coefficient of lift was compared. Total cells for the coarse grid is 343,105m,

while the total cells for the fine grid is 885,533. It is observed that the coefficient of lift for both the grids converged to the same value of 1.02 in this case. Since grid independency has already been established with the coarse grid, it was used for all other parametric studies.

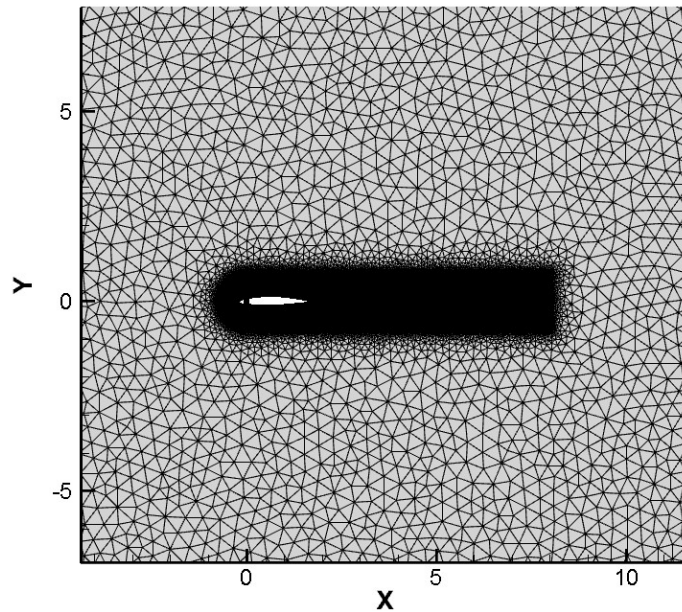


Figure 3-4 Fine grid

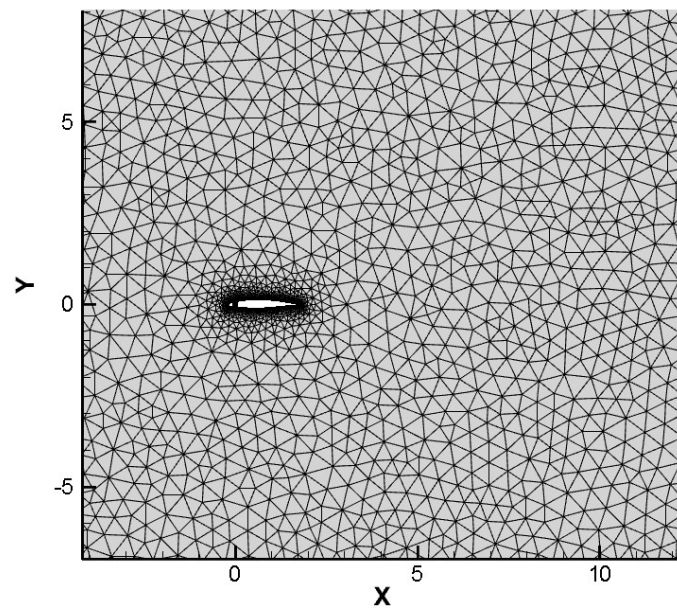


Figure 3-5 Coarse grid

### 3.2. Numerical Solver and Scheme

The commercial CFD solver, ANSYS Fluent, is employed to carry out the computations. The solver would implement finite volume discretization of 2-D Navier-Stokes incompressible equation along with turbulence models to generate pressure, velocity and temperature field throughout the domain. The 2-D Navier-Stokes equation is given below.

#### Continuity Equation

$$\frac{\delta u_x}{\delta x} + \frac{\delta u_y}{\delta y} = 0$$

#### Momentum Equation

$$\frac{\delta u_x}{\delta t} + u_x \frac{\delta u_x}{\delta x} + u_y \frac{\delta u_x}{\delta y} = -\frac{1}{\rho} \frac{\delta p}{\delta x} + \nu \frac{\delta^2 u_x}{\delta x^2} + \nu \frac{\delta^2 u_x}{\delta y^2}$$

$$\frac{\delta u_y}{\delta t} + u_x \frac{\delta u_y}{\delta x} + u_y \frac{\delta u_y}{\delta y} = -\frac{1}{\rho} \frac{\delta p}{\delta y} + \nu \frac{\delta^2 u_y}{\delta x^2} + \nu \frac{\delta^2 u_y}{\delta y^2}$$

#### Energy Equation

$$\rho \frac{D}{Dt} \left( e + \frac{V^2}{2} \right) = \rho \dot{q} + \frac{\delta}{\delta x} \left( k \frac{\delta T}{\delta x} \right) + \frac{\delta}{\delta y} \left( k \frac{\delta T}{\delta y} \right) - \frac{\delta(u_x p)}{\delta x} - \frac{\delta(u_y p)}{\delta y} + \frac{\delta(u_x \tau_{xx})}{\delta x} + \frac{\delta(u_x \tau_{yx})}{\delta y} + \frac{\delta(u_y \tau_{xy})}{\delta x} + \frac{\delta(u_y \tau_{yy})}{\delta y}$$

where  $u_x$  is the x-component of velocity,  $u_y$  is the y-component of velocity,  $t$  is time,  $\rho$  is density,  $p$  is static pressure,  $\nu$  is kinematic viscosity,  $e$  is internal energy per unit mass,  $V$  is velocity of fluid per unit mass,  $T$  is temperature,  $k$  is thermal conductivity,  $\tau_{xx}$  is shear stress on x plane in x direction,  $\tau_{xy}$  is shear stress on x plane in y direction,  $\tau_{yx}$  is shear stress on y plane in x direction,  $\tau_{yy}$  is shear stress on y plane in y direction.

The simulations are ran at a fan rotation speed of 933 rad/s and Reynolds Number of  $3 \times 10^6$  where the characteristic length is taken as the chord length of the airfoil. Free-stream of Mach number of 0.07 approached the fan-wing model at  $0^\circ$  angle of attack. Time

step of 0.00035 seconds ensured that the blades did not make significant rotation in one time step. Unsteady 2<sup>nd</sup> order is applied with the turbulent intensity kept at 5%. Pressure-far-field boundary condition is implemented with Semi-Implicit Method for Pressure Linked Equations-Consistent (SIMPLEC) Scheme for Pressure-Velocity Coupling. The pressure far-field boundary condition is often called characteristic boundary condition, since it used characteristic information (Riemann invariants) to determine the flow variables at the boundaries. Second Order Upwind is used for energy, momentum, density, and second order for pressure. For turbulent kinetic energy and specific dissipation rate, first order upwind is implemented. Least square cell based method is used of the gradient.

## 4. Results and Analysis

The research started with simulations of a clean airfoil as shown in Figure 4-1 and parametric studies were carried out.



Figure 4-1 NACA 65<sub>1</sub>-212 Airfoil

Aerodynamic parameters such as coefficient of lift ( $C_l$ ), coefficient of drag ( $C_d$ ) and coefficient of power ( $C_p$ ) are calculated for the fan-wing cases and results were compared.

The coefficient of power ( $C_p$ ) is calculated as follows:

$$C_m = \frac{T_s}{\frac{1}{2} \rho u_\infty^2 c^2}$$

$$P = T_s \omega$$

$$C_p = \frac{P}{\rho \left(\frac{RPM}{60}\right)^3 D^5}$$

$C_m$  is the moment coefficient of the fan,  $T_s$  is torque required by the shaft to rotate the fan,  $\rho$  is the density of air,  $u_\infty$  is the velocity of freestream,  $c$  is the chord of the blades,  $P$  is the power required by the shaft to rotate the impeller,  $\omega$  is the rotational speed of the fan,  $D$  is diameter of the fan and  $C_p$  is coefficient of power.

### 4.1. Clean Case

Simulations are carried first carried out with a regular NACA 65<sub>1</sub>-212 airfoil with Reynolds number of  $3 \times 10^6$  and turbulent intensity of 5%. Various turbulence models are employed to help determine which turbulence model will be employed for the fan wing

cases. Figure 4-2 and Figure 4-3 shows the results of the clean case

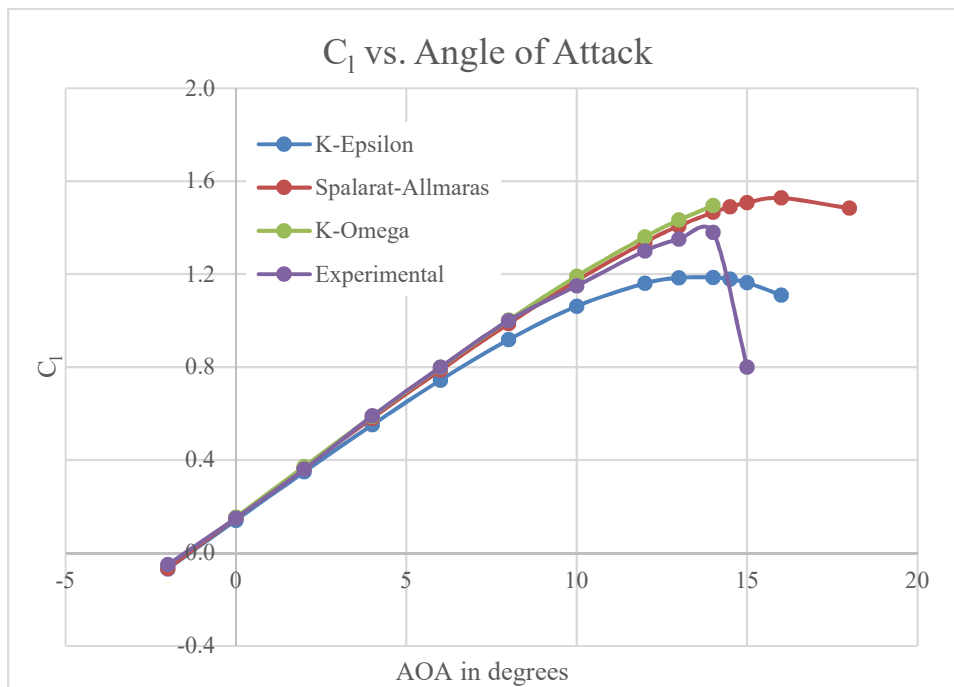


Figure 4-2 Coefficient of Lift vs. Angle of Attack

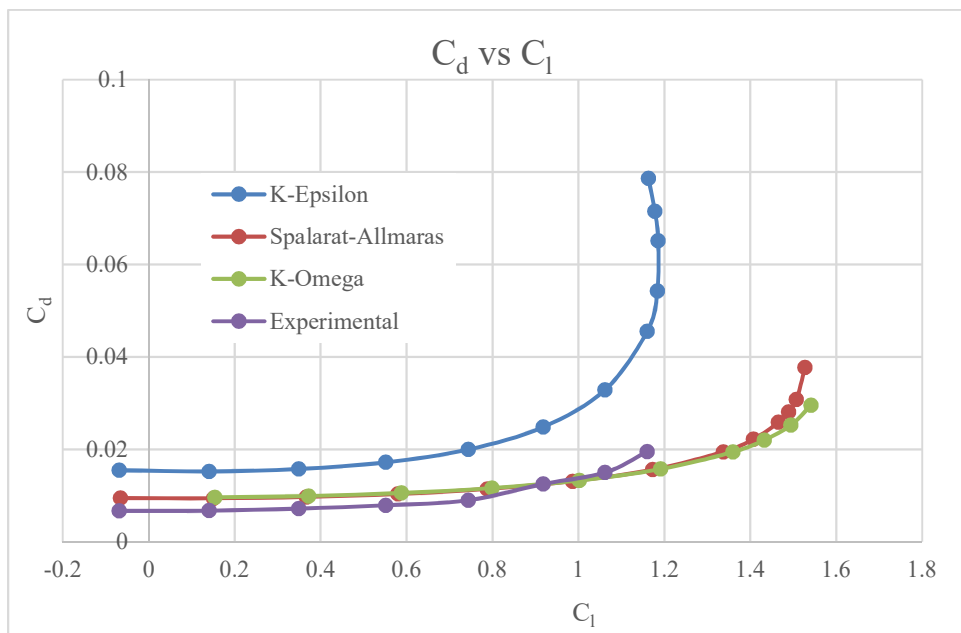


Figure 4-3 Coefficient of Drag vs Coefficient of Lift

The experimental data is obtained from NACA report (Abott, von Doenhoff, & Stivers, Jr., 1945). From the clean case results, it is determined that Spalart-Allmaras model

will be used for the parametric studies of the fan-wing model under the assumption that accuracy of results obtained in the clean case study will carry over to fan-wing study.

#### 4.2. Number of Blades

This set of simulations were carried out by changing the number of blades only. The bottom slat is set at 0.5in radius, the top slat is set to the original ratio of 1, hub-to-shroud ratio is set at 74% and blade pitch angle is set at 13 degrees.

Changing the number of blades is a trade-off between transfer of energy from the impeller to the kinetic energy of the air and the friction between the blades. As the number of blades increases the transfer of energy increases but the friction between the blades also increases. As a result, there should be an optimum point where the ratio of energy transfer to friction is maximum, which would be indicated by maximum circulation control. The following table and graphs shows the results of the simulations.

Table 4-1 Results from Number of Blades Study

Number of Blades	$C_l$	$C_d$	$C_p$	$C_l/C_p$
Experimental (No blades)	0.150	0.005		
36 blades	0.912	-0.193	0.333	2.739
30 blades	0.952	-0.255	0.348	2.736
26 blades	0.988	-0.327	0.356	2.776
25 blades	0.992	-0.312	0.355	2.796
24 blades	1.020	-0.316	0.351	2.906
23 blades	0.982	-0.358	0.356	2.758
22 blades	0.975	-0.368	0.349	2.794



Number of Blades	$C_l$	$C_d$	$C_p$	$C_l/C_p$
20 blades	0.957	-0.391	0.344	2.782
10 blades	0.648	-0.142	0.213	3.036

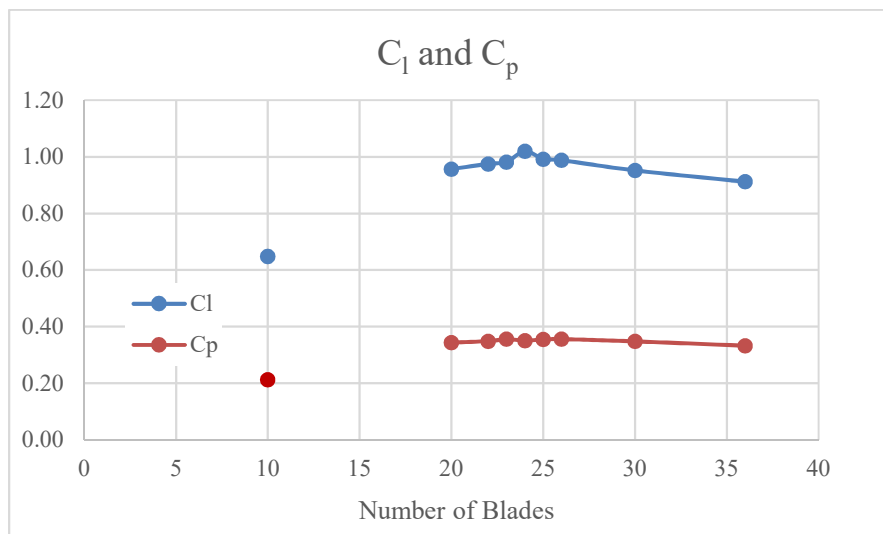


Figure 4-4  $C_l$  and  $C_p$  vs. Number of Blades

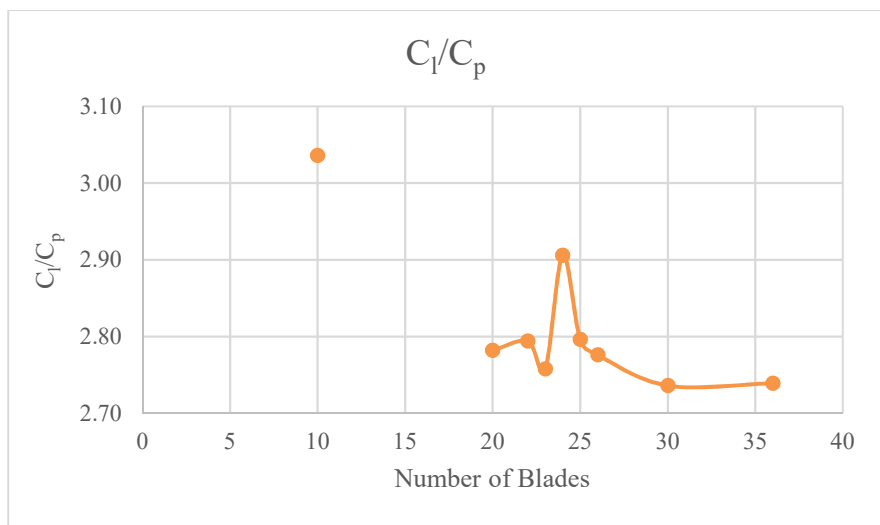


Figure 4-5  $C_l/C_p$  vs. Number of Blades

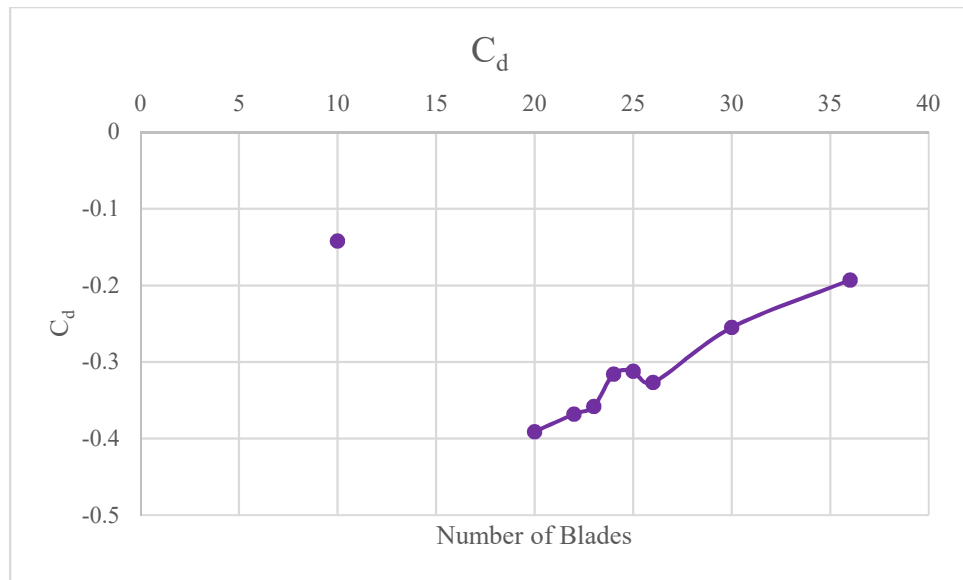


Figure 4-6  $C_d$  vs. Number of Blades

From Figure 4-4, it is observed that the maximum circulation control is achieved with 24 blades and the power required by the shaft to turn the impeller remains close to each other from 24 blades onwards.

From Figure 4-6, it is observed that number of blades of 20-23 generates more thrust than 24 blades. Comparing with the circulation control data, this thrust generation is unexpected however the wall shear stress of 24 blades and 22 blades is analyzed to understand this phenomenon as shown in Figure 4-7. The shear stress on the airfoil surrounding the fan region caused by 24 blades is higher than 22 blades, causing the system with 24 blades to have more drag hence less thrust.

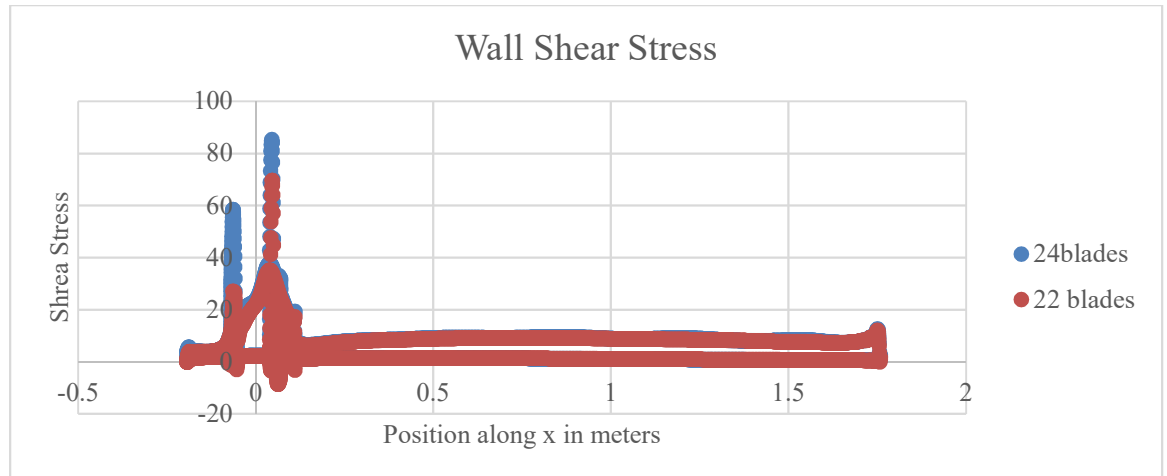


Figure 4-7 Wall Shear Stress between 24 Blades and 22 Blades

### 4.3. Blade Pitch Angle

This set of simulations were carried out by changing the blade pitch angle only. The bottom slat is set at 0.5in radius, the top slat is set to the original ratio of 1, hub-to-shroud ratio is set at 74% and number of blades is kept at 24. Figure 4-8 indicates the blade pitch angle. It is expected that a certain angle maximum amount of air would be able to exit the fan efficiently. A lower value of pitch angle would make the blade straight, and the through flow of the fan would hit the nose of the airfoil while exiting the fan causing the flow to slow down and increasing the drag. A higher value of blade pitch angle would make the blades more curved causing more air to enter into the circulation flow and not exit the fan causing more drag and less efficiency.

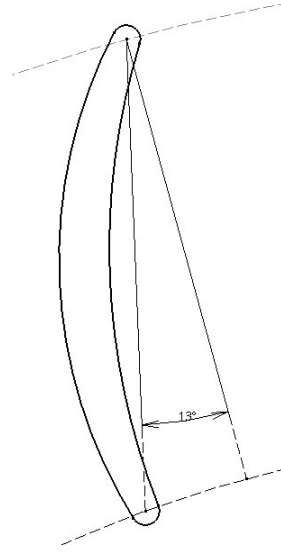


Figure 4-8 Blade Pitch Angle

Table 4-2 Results from Blade Pitch Angle Study

Pitch Angle (degrees)	$C_i$	$C_d$	$C_p$	$C_i/C_p$
5	0.859	-0.666	0.409	2.098
9	0.965	-0.536	0.382	2.524
11	0.987	-0.457	0.370	2.665
13	1.020	-0.316	0.351	2.904
17	0.906	-0.115	0.311	2.910
21	0.762	0.079	0.258	2.951
25	0.655	0.201	0.237	2.765

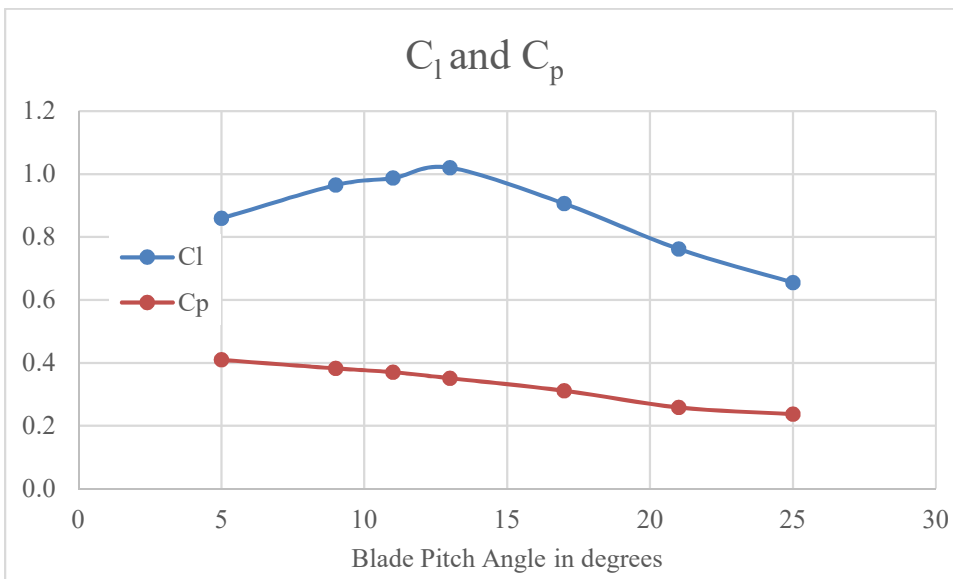


Figure 4-9 C<sub>l</sub> and C<sub>p</sub> vs. Blade Pitch Angle

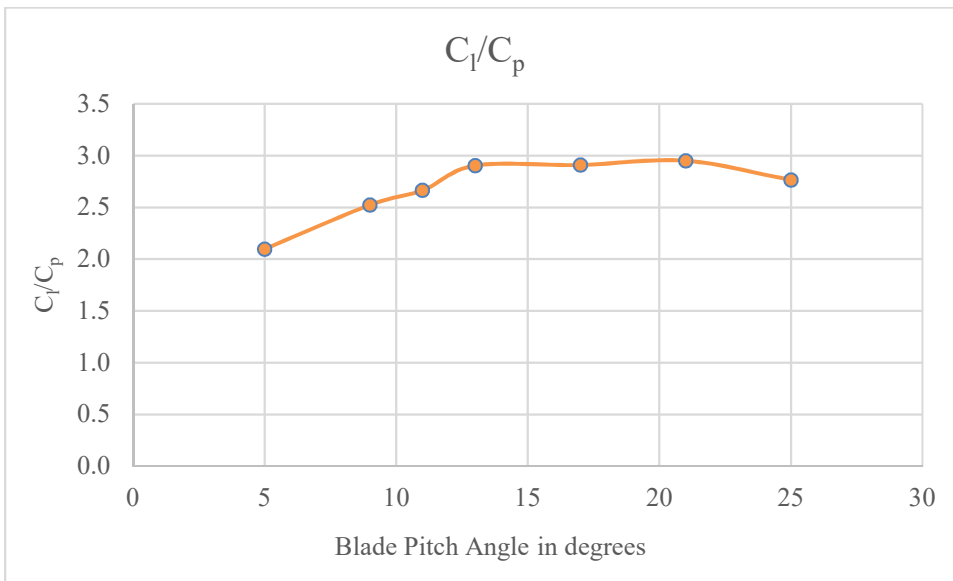


Figure 4-10 C<sub>l</sub>/C<sub>p</sub> vs. Blade Pitch Angle

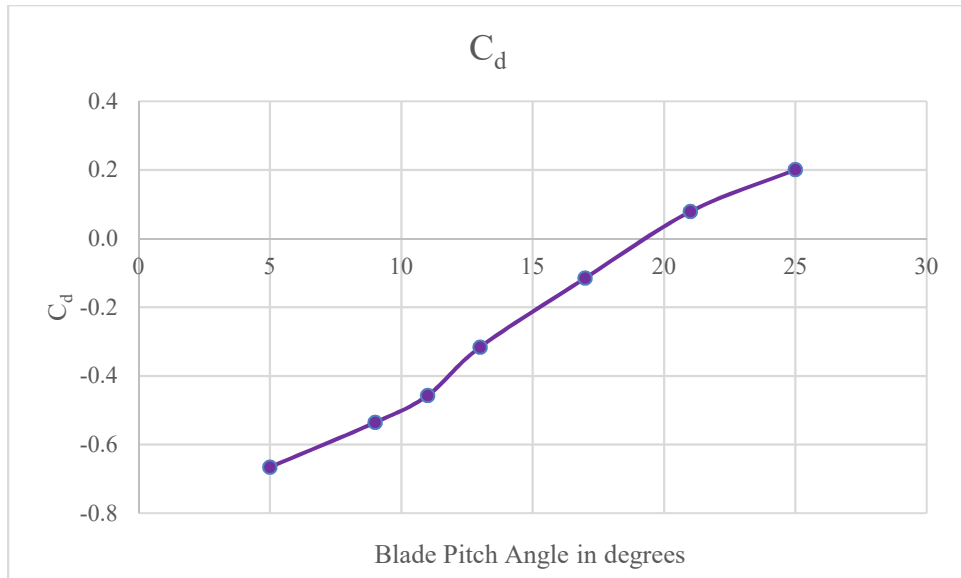


Figure 4-11 C<sub>d</sub> vs. Blade Pitch Angle

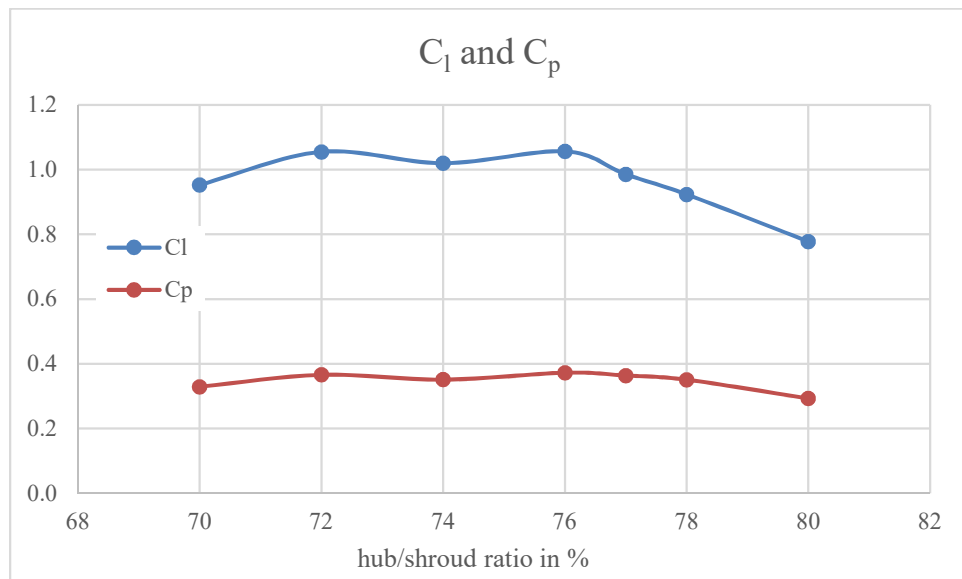
It is observed that a maximum lift is obtained at blade pitch angle of 13°, yielding a higher value of thrust as expected.

#### 4.4. Fan Diameter Ratio

This set of simulations were carried out by changing the hub-to-shroud only. The bottom slat is set at 0.5in radius, the top slat is set to the original ratio of 1, blade pitch angle is set at 13 degrees and number of blades is kept at 24. It is expected a certain fan diameter ratio would yield the highest circulation control. A higher ratio value would mean the blades are smaller hence energy from the shaft cannot efficiently transfer to through flow, whereas a lower ratio value would mean the blades are bigger than necessary causing generating higher friction and slowing down the through flow and hence the lift generated.

Table 4-3 Results from Fan Diameter Ratio Study

d/D (%)	$C_l$	$C_d$	$C_p$	$C_l/C_p$
70	0.953	-0.163	0.329	2.897
72	1.055	-0.321	0.366	2.885
74	1.020	-0.315	0.351	2.906
76	1.057	-0.486	0.372	2.838
77	0.986	-0.478	0.364	2.711
78	0.923	-0.415	0.351	2.633
80	0.778	-0.311	0.293	2.655

Figure 4-12  $C_l$  and  $C_p$  vs. Hub/Shroud Ratio

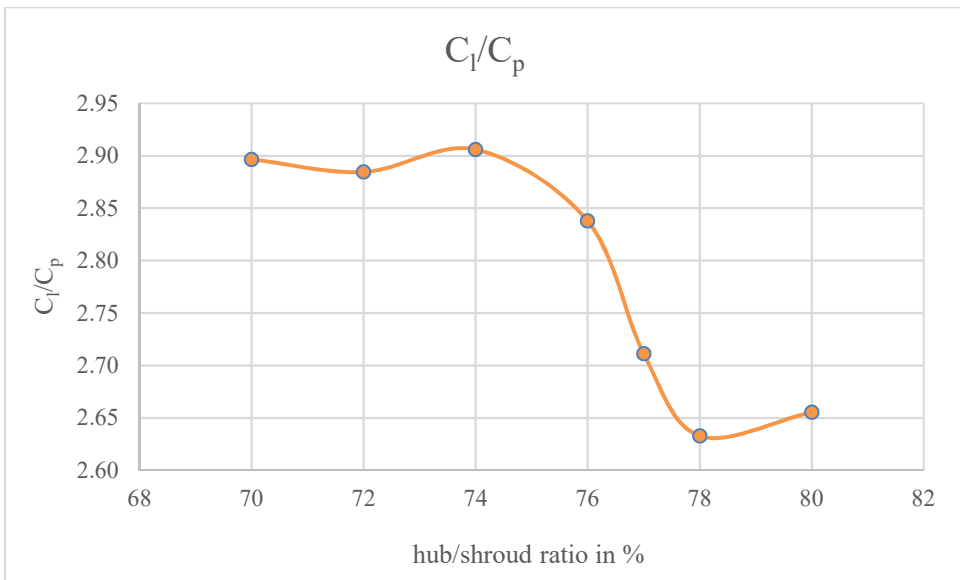


Figure 4-13  $C_1/C_p$  vs Hub/Shroud Ratio

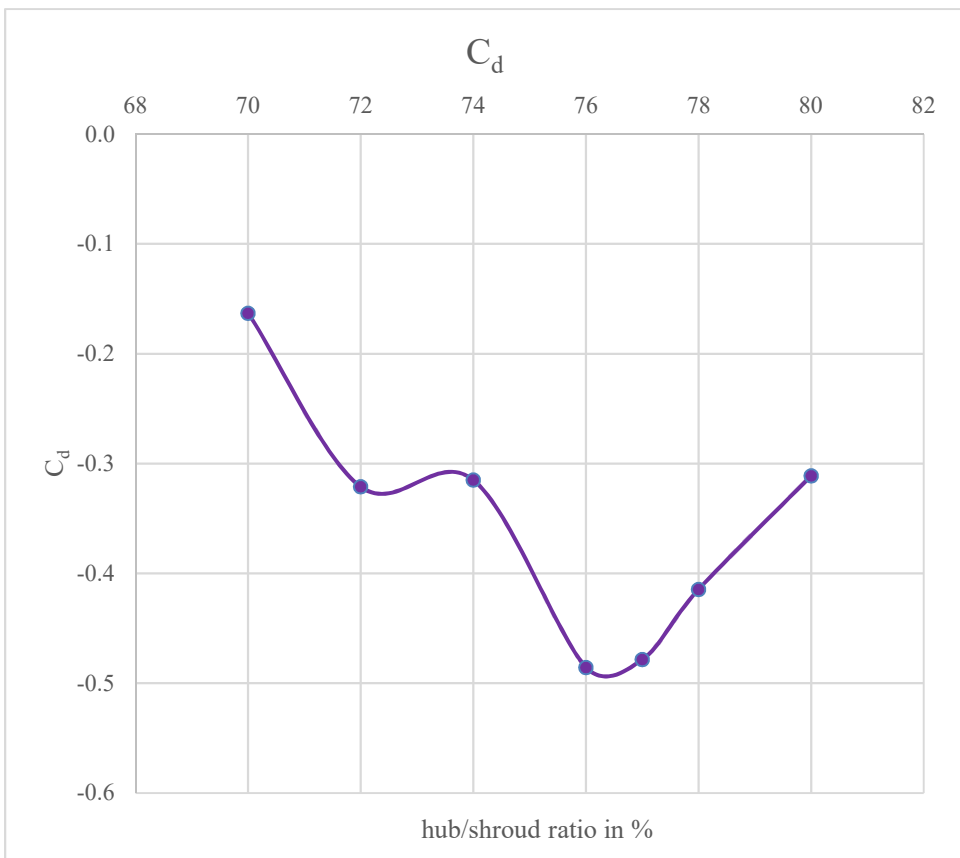


Figure 4-14  $C_d$  vs Hub/Shroud Ratio



The results from this study yielded a strange phenomenon as the value of  $C_i$  has two peaks. Analyzing the value of  $C_d$  between two peaks indicates that the 76% is more beneficial as it generates more thrust.

#### 4.5. Pressure Side Slat Opening

This set of simulations were carried out by changing bottom slat opening only. The hub-to-shroud ratio is kept at 74%, the top slat is set to the original ratio of 1, blade pitch angle is set at 13 degrees and number of blades is kept at 24. Figure 4-15 indicates the bottom slat opening, changing the radius changes the size of the opening.

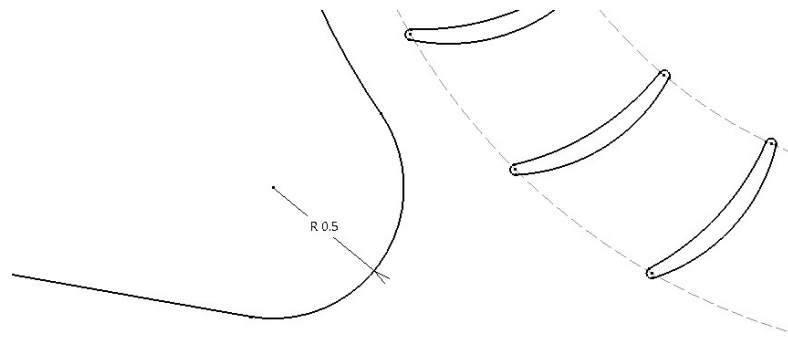


Figure 4-15 Pressure Side Slat Opening

Table 4-4 Results from Bottom Slat Opening Study

Slat Radius (in)	$C_i$	$C_d$	$C_p$	$C_i/C_p$
0.4	0.986	-0.360	0.359	2.747
0.5	1.020	-0.361	0.351	2.906
0.7	0.943	-0.278	0.331	2.845

Slat Radius (in)	$C_l$	$C_d$	$C_p$	$C_l/C_p$
1	0.892	-0.182	0.298	2.994
1.2	0.846	-0.178	0.284	2.981
1.5	0.819	-0.155	0.267	3.073
1.7	0.781	-0.118	0.244	3.204
2	0.781	-0.112	0.246	3.173

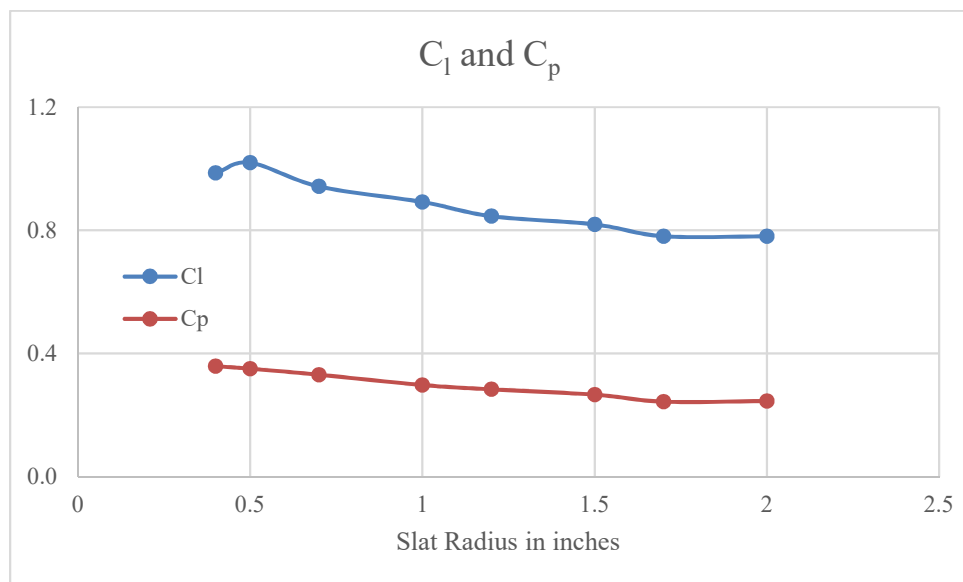
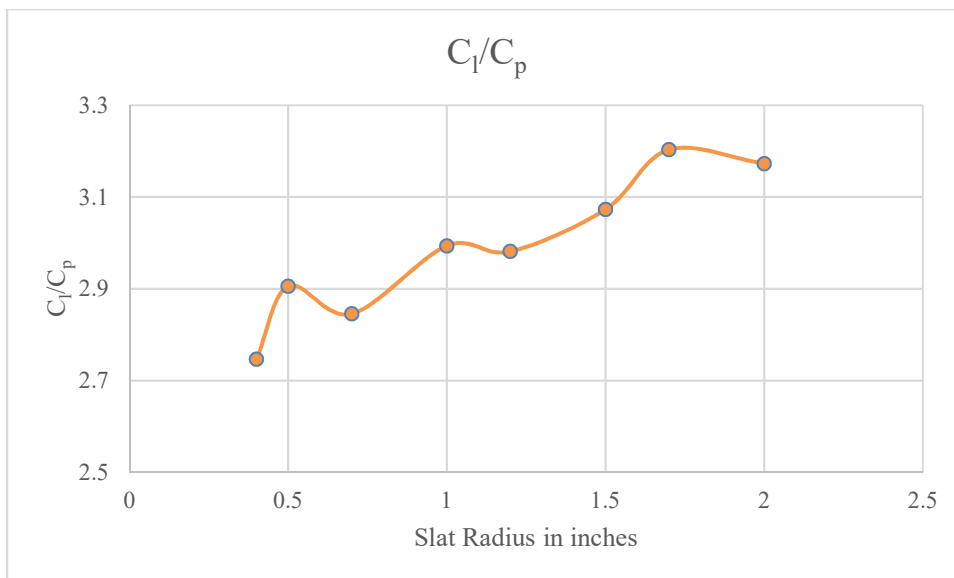
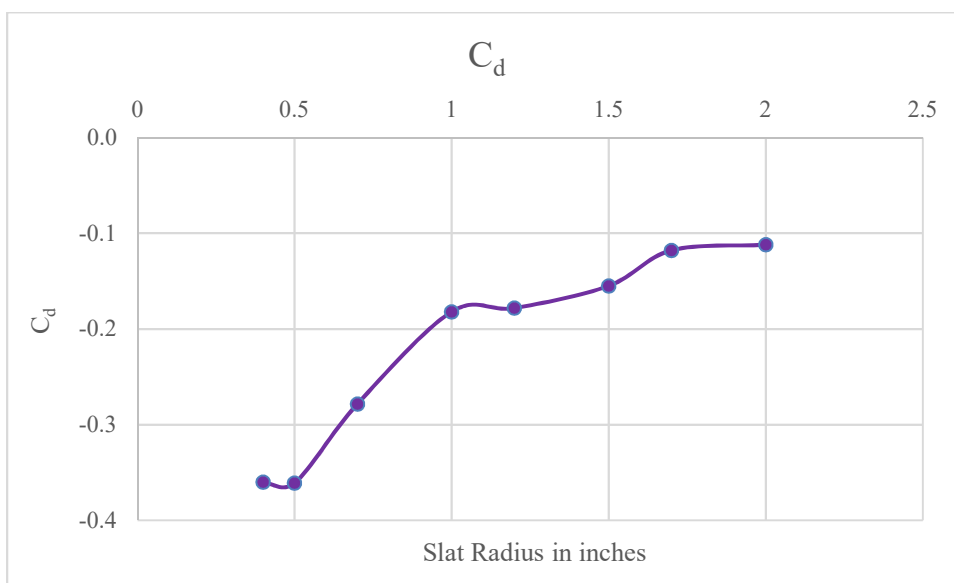


Figure 4-16  $C_l$  and  $C_p$  vs. Slat Radius

Figure 4-17  $C_l/C_p$  vs Slat RadiusFigure 4-18  $C_d$  vs/ Slat Radius

It is observed that a slat radius of 0.5 inches yielded the highest  $C_l$ . Any value other than 0.5 inches caused the incoming to slow down to rate of mass flow and friction at the inlet which in turned slowed down the exit jet from the fan.

#### 4.6. Suction Side Slat Opening

This set of simulations were carried out by changing the top slat opening only. The bottom slat is set at 0.5in radius, the hub-to-shroud ratio is kept at 74%, blade pitch angle is set at 13 degrees and number of blades is kept at 24. The top slat opening is changed by stretching the y coordinates from Figure 2-1. It is expected at a certain point the optimum circulation control would be achieved. A lower than ideal value would make the opening the narrower where the boundary layers of the airfoil and nose would interact with each other causing the flow to slow down and a higher than ideal value would work like a divergent nozzle slowing the flow decreasing the circulation control.

Table 4-5 Results from Top Slat Opening Study

Stretch Factor	$C_l$	$C_d$	$C_p$	$C_l/C_p$
0.90	0.760	-0.157	0.203	3.744
0.95	0.872	-0.233	0.253	3.447
1.00	1.020	-0.315	0.351	2.906
1.05	1.035	-0.349	0.423	2.449
1.10	0.997	-0.356	0.464	2.149
1.15	0.949	-0.330	0.525	1.809

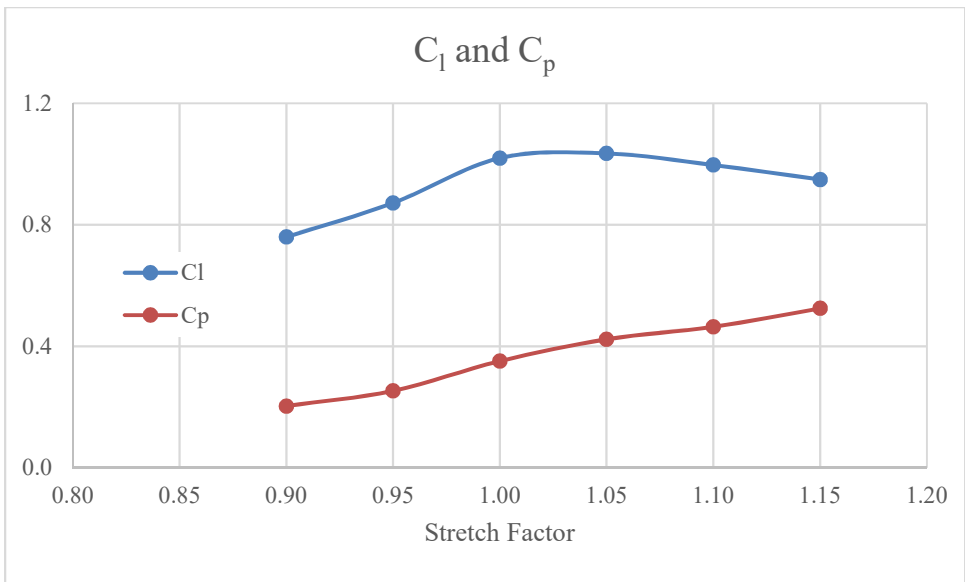


Figure 4-19  $C_l$  and  $C_p$  vs. Stretch Factor

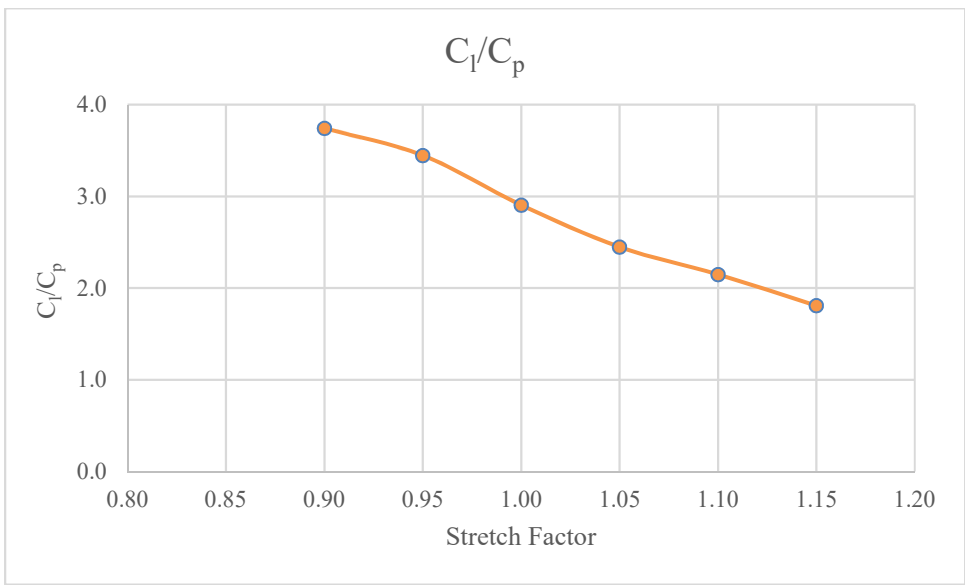


Figure 4-20  $C_l/C_p$  vs. Stretch Factor

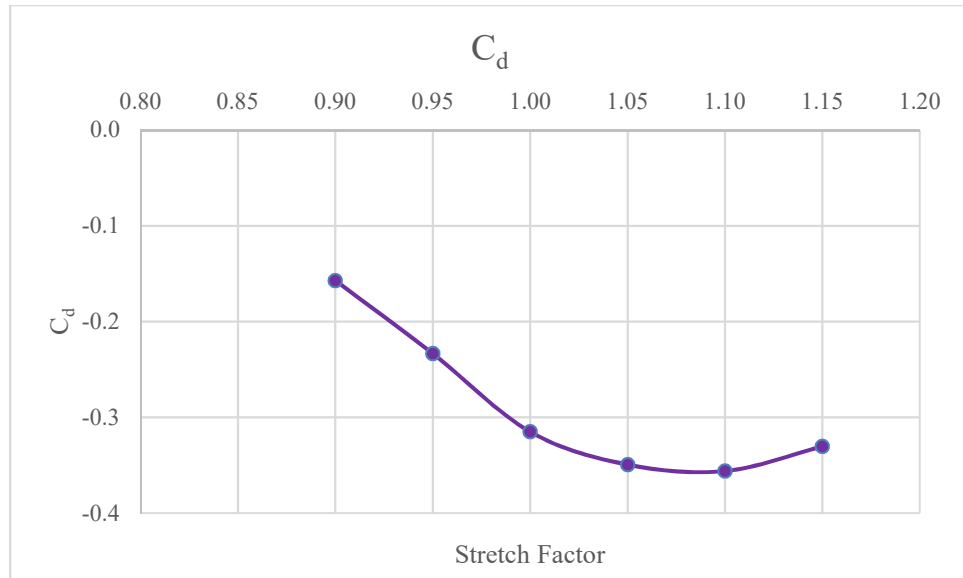


Figure 4-21  $C_d$  vs. Stretch Factor

It is observed that a top slat opening of 1.05 yielded the maximum circulation control, while generating the highest thrust generated in the group as well.

#### 4.7. Regression Analysis

All the parametric studies done so far was by changing one variable and keeping rest of the parameters constant. While this parametric study illustrates the type of relationship between the aerodynamic parameters and the parameter studied, a change in value in one of the parameter which was kept constant would result in different values from the parametric study. For example, in number of blades cases,  $C_1$  of 1.02 is obtained with 24 blades and keeping top slat opening at 1, bottom slat opening at 0.5 inches, blade pitch angle at  $13^\circ$  and hub-to-shroud ratio at 74%. In a case where hub-to-shroud ratio is set to something other 74%, while doing the number of blades study will not yield  $C_1$  of 1.02 with 24 blades, as the variables are interdependent to each other.

In order to optimization, an objective function is necessary. However, the research so far has yielded only data, hence regression analysis is carried out on the acquired set of data in order to find the best objective function from which optimization can be carried out. The regression analysis combine all the parameters in one equation of lift. Critical points of that equation gives the combination of parameters which would give a higher value of circulation control than achieved by individual parametric study.

Linear regression model is neglected as the graphs of  $C_l$  and the parameters did not yield a liner looking relationship. A quadratic equation was first established and analyzed. The equation below shows the relationship between  $C_l$  and the parameters.

$$C_l = An^2 + Bn + Cx^2 + Dx + Ey^2 + Fy + Gz^2 + Hz + Id^2 + Jd + \beta$$

where  $A, B, C, D, E, F, G, H, I, J$  and  $\beta$  are constants that needs to be calculated and  $n$  is the number of blades,  $x$  is the bottom slat opening,  $y$  is the top slat opening,  $z$  is the blade pitch angle and  $d$  is the hub-to-shroud ratio.

The regression analysis yielded an  $r^2$  value of 0.96, which can be accepted as a sufficient measure of how close the given data fits the regression equation. The values of coefficients obtained are given below:

Table 4-6 Coefficients from regression equation

$A = -0.00113$	$B = 0.06125$
$C = -0.00711$	$D = -0.10768$
$E = -9.78139$	$F = 20.74778$
$G = -0.00211$	$H = 0.05075$
$I = -38.88078$	$J = 56.57118$
$\beta = -31.62775$	

The objective equation generated using the regression analysis was compared with the computational data acquired so observe whether the objective equation replicates the data from CFD. If it does then the critical points obtained from the regression equation can be expected to yield an optimum solution of thrust control.

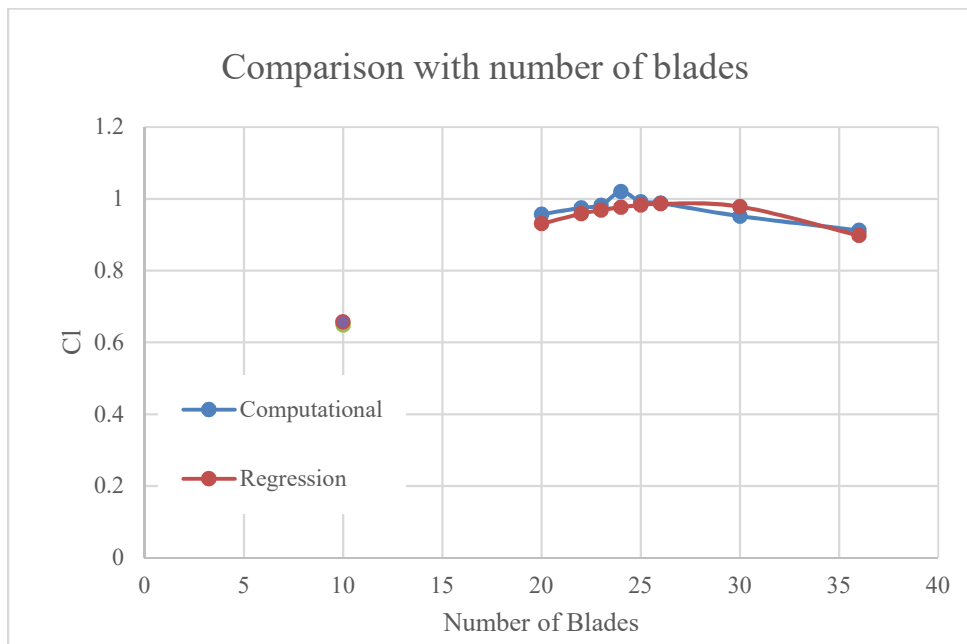


Figure 4-22 Comparison with number of blades data

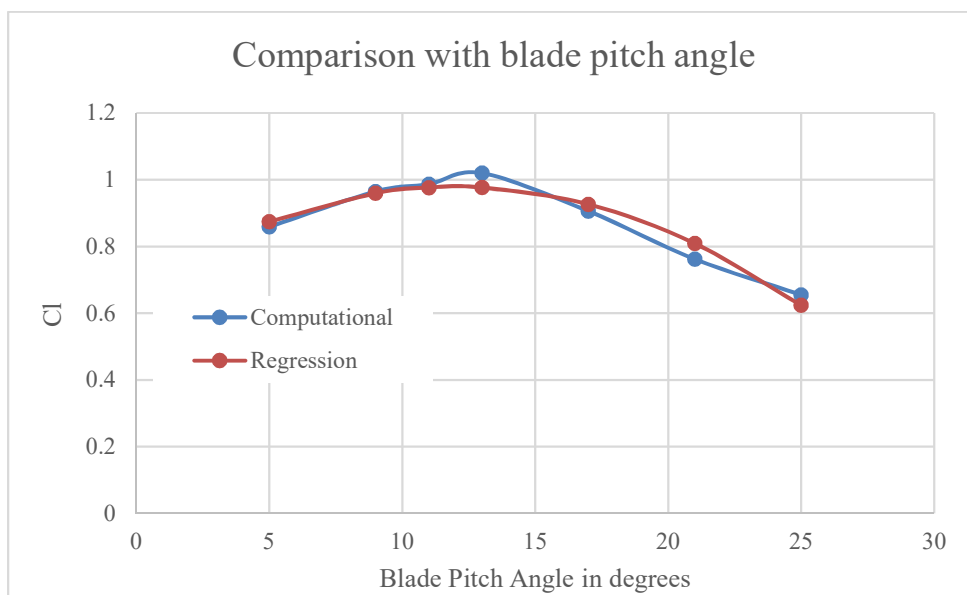


Figure 4-23 Comparison with blade pitch angle data



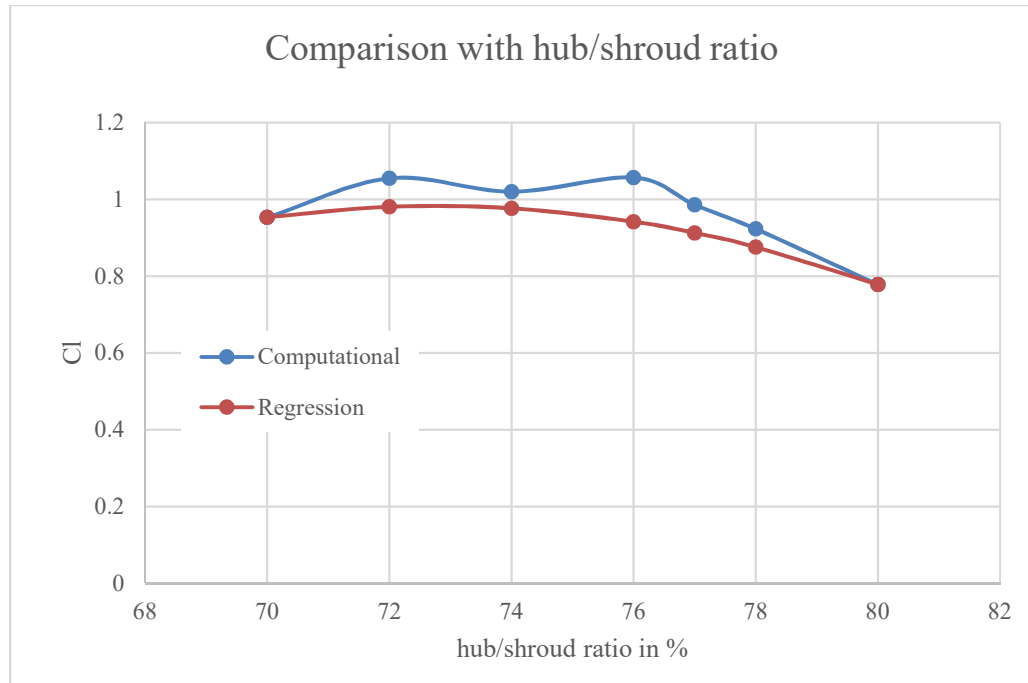


Figure 4-24 Comparison with hub/shroud ratio data

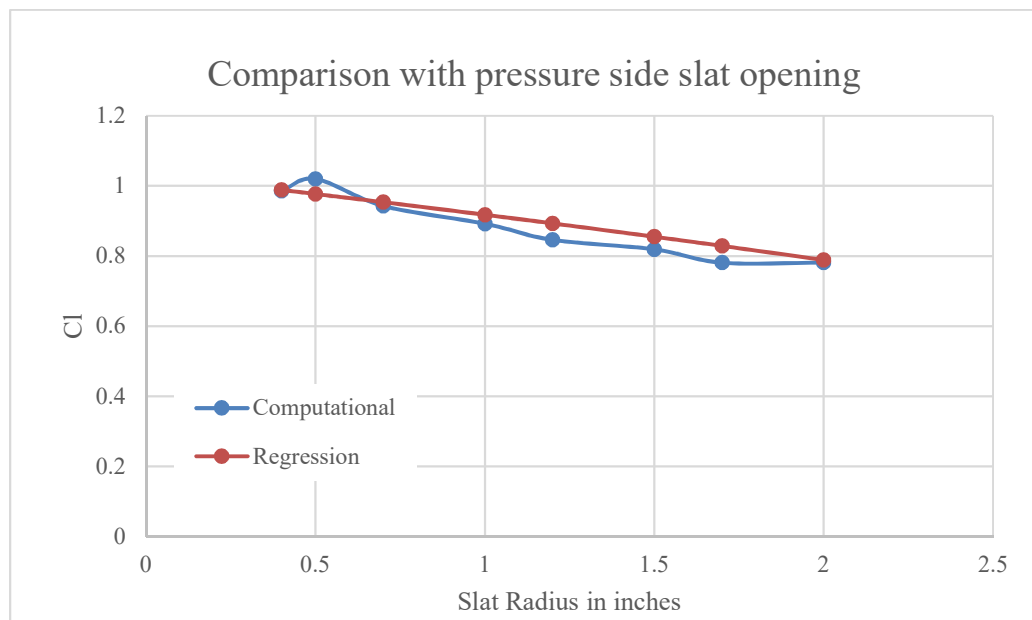


Figure 4-25 Comparison with pressure side slat opening data

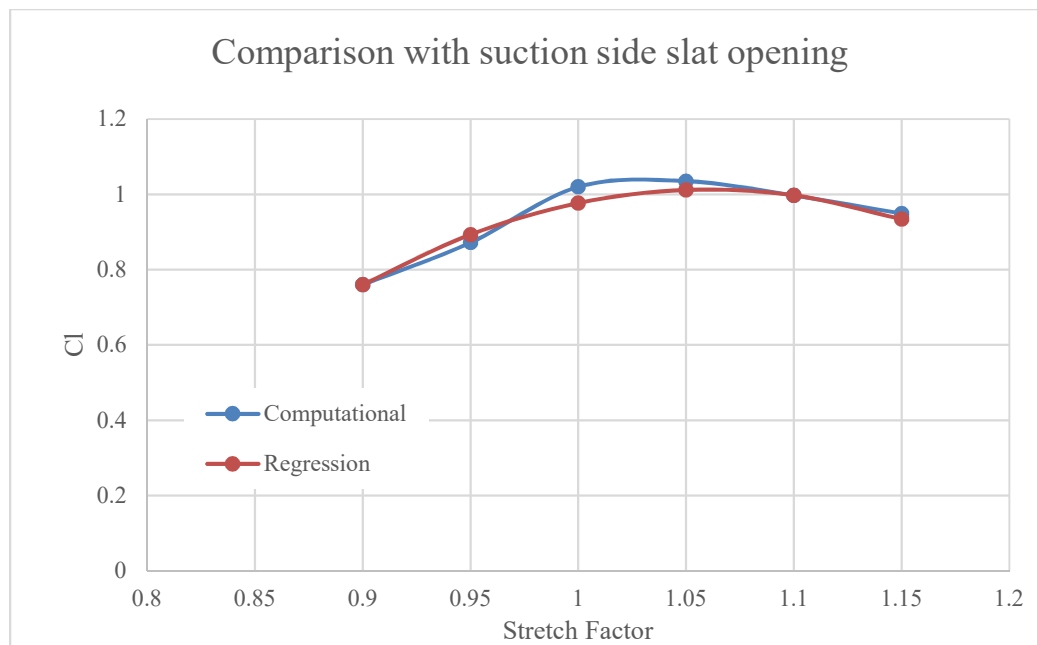


Figure 4-26 Comparison with suction side slat opening data

It is observed that the regression analysis yielded an objective function that correlates with the computational data generated in this research. This objective function can then be used for optimization for circulation control.

From the values of the coefficients, critical points were established by taking the first derivative of the regression equation.

Table 4-7 Critical Points obtained from Regression Analysis

n	27.044
x	-7.57
y	1.0605
z	12.0506
d	72.75%

It is noticed that the bottom slat opening yielded a negative critical point which is not physically possible in the fan-wing model. Hence, while creating the grid using this combination of parameters, bottom slat opening was kept at 0.5 inches which was originally used. Simulation was run using the same boundary conditions and angular velocity of the fan and the results were analyzed.

Table 4-8 Results obtained from simulation from regression analysis parameters

$C_l$	$C_d$	$C_p$	$C_l/C_p$
1.11	-0.387	0.454	2.424

It is noted that running the fan at 933 rad/s on this combination of parameters yielded the highest value of  $C_l$  obtained in the research. However correspondingly the thrust generated is not the highest as the friction of blades increased drag. The regression equation combined the parameters into a single equation of circulation control, hence the combination of parameters yielded a higher value of lift running at the same conditions. However, the other aerodynamic parameters were not optimum as they were not considered in the regression analysis.

An exponential equation of third order was also attempted, but the critical point of the bottom slat opening came out to be a complex number and that equation was aborted. Any equation of higher order than 3 generated significant error while calculating the coefficients, hence they were aborted as well.

The second order objective function generated here is similar to the response surface methodology which is also a second-degree polynomial model. However the method used in this research is more flexible as the order of the polynomial can be individually set while carrying out the regression analysis.

#### 4.8. Effect of Thickness on Circulation Control

The thin NACA 65<sub>1</sub>-212 was chosen for this research so that it can be compared with Karpuk's data where a thick NACA 65(3)-221 was implemented (Karpuk, Kazarin, Gudmundsson, & Golubev, 2018). The data is compared with the same power rating for both the cases, since a smaller fan would rotate faster at the same power rating compared to a larger fan.

Table 4-9 Comparison between thick and thin airfoil

	Clean Case $C_l$	CFF $C_l$	Ratio Increase
<b>NACA 65(3)-221</b>	0.2	1.5	7.5
<b>NACA 65<sub>1</sub>-212</b>	0.15	1.1	7.33

As it can be seen that the ratio increase due to the embedded cross flow fan is almost similar for both the airfoil. It can be concluded that the percentage of circulation control gained is independent of the thickness of the airfoil used. However for absolute increase in circulation control a thicker airfoil is better suited.

## 5. Conclusion

A concept of a cross-flow fan embedded near the leading edge of an airfoil to actively control the boundary layer for lift and thrust enhancement has been studied computationally. The design places a cross-flow fan near the leading edge of an airfoil and flow is drawn in from the pressure side of the airfoil, energized and expelled out to the suction side near the leading edge. The effect of number of blades, blade pitch angle, fan diameter ratio, pressure side slat opening and suction side slat opening have on aerodynamic parameters have been investigated. It is observed from the number of blades study that 24 number of blades generated the maximum circulation control, from the blade pitch angle study  $13^\circ$  was the blade pitch angle which yielded the maximum circulation control, 76% hub-to-shroud ratio generated the maximum lift from that group of study, bottom slat opening radius of 0.5 inches and top slat opening factor of 1.05 yielded the maximum circulation control. Regression analysis on the acquired set of data indicated that a second order exponential equations generated an acceptable fit equation from which the combination of 27 number of blades, 0.5 inches pressure side slat opening, suction side slat opening factor of 1.0605, blade pitch angle of  $12.051^\circ$  and hub-to-shroud ratio of 72.75% generated the highest lift obtained in the study. Although it cannot be said for certain that this combination yielded the highest lift possible.

## 6. Recommendations

A more detailed grid sensitivity analysis should be carried out to clearly indicate at which point grid independency is reached. Time step sensitivity analysis and spatial sensitivity analysis should be rigorously performed to better determine at what point time step independency and spatial independency is reached

A more detailed analysis using various turbulence models for the fan-wing cases would indicate which turbulence model is better than the other when experimental data is made available to be compared with.

A further development of the regression analysis where complex functions and constrained parameters are employed to understand the relationship between lift and the parameters involved would provide a better combination of parameter which would provide a greater circulation control. The One-Factor-at-a-Time (OFAT) was implemented in this computational study to gather knowledge. Since OFAT is considered inefficient, more randomization in the design of experiments can be considered for future study. Regression analysis can also be done with to optimize for power or thrust.

## REFERENCES

- Abott, H. I., von Doenhoff, E. A., & Stivers, Jr., S. L. (1945). *Report No. 824*. Langley Field: National Advisory Committee for Aeronautics.
- Chawla, K. (1984). *Optimization of Cross Flow Fan Housing for Airplane Wing Installation*. Arlington: University of Texas at Arlington.
- Dang, T. Q., & Bushnell, P. R. (2009). Aerodynamics of Cross-Flow Fans and their Application to Aircraft Propulsion and Flow Control. *Progress in Aerospace Sciences*, 1-29.
- Dornier, P. (1962). *USA Patent No. 3,065,928*.
- Hancock, J. (1980). Tests of a High Efficiency Transverse Fan. *AIAA/SAE/ASME 16th Joint Propulsion Conference*. Hartford, Connecticut: AIAA-80-143.
- Jimenez, J. (2013). *Free Shear Flows*. Madrid: Universidad Politecnica de Madrid. Retrieved from torroja.dmt.upm.es.
- Jones, A. (2013). *Integration of Twenty-Bladed Cross-Flow Fan into Vertical Take-Off and Landing*. Monterey: Naval Postgraduate School.
- Karpuk, S. V., Kazarin, P., Gudmundsson, S., & Golubev, V. V. (2018). Preliminary Feasibility Study of a Multi-Purpose Aircraft Concept with a Leading-Edge Embedded Cross-Flow Fan. *AIAA SciTech Forum*. Kissimmee: American Institute of Aeronautics and Astronautics, Inc.
- Kim, J.-W., Ahn, E. Y., & Oh, H. W. (2005). Performance Prediction of Cross-Flow Fans Using Mean Streamline Analysis. *International Journal of Rotating Machinery*, 112-116.
- Kummer, J. (2006). *Simulation of the Cross-Flow Fan and Application to a Propulsive Airfoil Concept*. Syracuse: Syracuse University.
- Lin, C.-H. (1986). *A Wind Tunnel Investigation of the External Aerodynamics of an Airfoil with an Internal Cross Flow Fan*. Arlington: University of Texas at Arlington.
- Mortier, P. (1893). *France Patent No. US507445*.
- Nieh, T.-W. (1988). *The Propulsive Characteristics of a Cross Flow Fan Installed in an Airfoil*. Arlington: University of Texas at Arlington.
- Schlichting, H., & Glaus, K. (2017). *Boundary-Layer Theory*. Berlin: Springer-Verlag.
- Toffolo, A. (2004). On Cross-Flow Fan Theoretical Performance and Efficiency Curves:

An Energy Loss Analysis on Experimental Data. *Journal of Fluids Engineering*.

TRANE. (2000). WASG Engineering Technology. *Air Moving Technology Seminar* (pp. 10.8-10.9). Wichita: American Standard Companies.